AD-A092 909 DAYTON UNIV OH RESEARCH INST F/G 1/3
EVALUATION OF BIRD LOAD MODELS FOR DYNAMIC ANALYSIS OF AIRCRAFT--ETC(U)
AUG 80 B S WEST, R A BROCKMAN F33615-76-C-3103
UNCLASSIFIED UDR-TR-80-59 AFWAL-TR-80-3092 NL

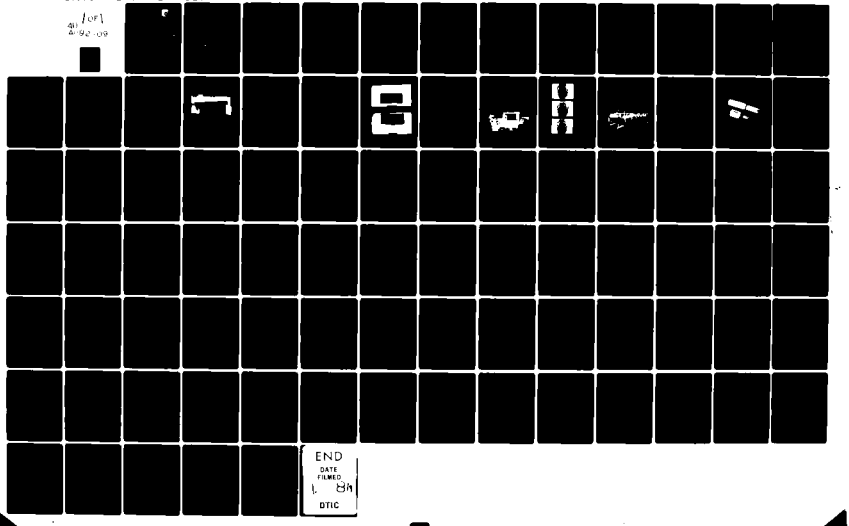

AFWAL-TR-80-3092

AD A092909

LEVEL II

EVALUATION OF BIRD LOAD MODELS FOR DYNAMIC ANALYSIS OF AIRCRAFT TRANSPARENCIES

BLAINE S. WEST
ROBERT A. BROCKMAN
UNIVERSITY OF DAYTON RESEARCH INSTITUTE
DAYTON, OHIO 45469

AUGUST 1980

TECHNICAL REPORT AFWAL-TR-80-3092
Final Report for Period January 3, 1978 — December 1979

Approved for public release; distribution unlimited.

FLIGHT DYNAMICS LABORATORY
AIR FORCE WRIGHT AERONAUTICAL LABORATORIES
AIR FORCE SYSTEMS COMMAND
WRIGHT-PATTERSON AIR FORCE BASE, OHIO 45433

NOTICE

When Government drawings, specifications, or other data are used for any purpose other than in connection with a definitely related Government procurement operation, the United States Government thereby incurs no responsibility nor any obligation whatsoever; and the fact that the government may have formulated, furnished, or in any way supplied the said drawings, specifications, or other data, is not to be regarded by implication or otherwise as in any manner licensing the holder or any other person or corporation, or conveying any rights or permission to manufacture use, or sell any patented invention that may in any way be related thereto.

This report has been reviewed by the Office of Public Affairs (ASD/PA) and is releasable to the National Technical Information Services (NTIS). At NTIS, it will be available to the general public, including foreign nations.

This technical report has been reviewed and is approved for publication.

Robert E. McCarty
Project Engineer

R. Harley Walker
Group Leader
Subsystems Development Group

FOR THE COMMANDER

Ambrose B. Nutt
Director
Vehicle Equipment Division

"If your address has changed, if you wish to be removed from our mailing list, or if the addressee is no longer employed by your organization please notify AFWAL/FIER, WPAFB, OH 45433 to help us maintain a current mailing list."

Copies of this report should not be returned unless return is required by security considerations, contractual obligations, or notice on a specific document.

AIR FORCE/56780/30 October 1980 — 200

Unclassified

SECURITY CLASSIFICATION OF THIS PAGE (When Data Entered)

REPORT DOCUMENTATION PAGE	READ INSTRUCTIONS BEFORE COMPLETING FORM
1. REPORT NUMBER: AFWAL-TR-80-3092	2. GOVT ACCESSION NO.: AD-A092 909
3. RECIPIENT'S CATALOG NUMBER:	
4. TITLE (and Subtitle): EVALUATION OF BIRD LOAD MODELS FOR DYNAMIC ANALYSIS OF AIRCRAFT TRANSPARENCIES	5. TYPE OF REPORT & PERIOD COVERED: Final Report for Period Jan 1978-Dec 1979
	6. PERFORMING ORG. REPORT NUMBER: UDR-TR-80-59
7. AUTHOR(s): Blaine S. West, Robert A. Brockman	8. CONTRACT OR GRANT NUMBER(s): F33615-76-C-3103
9. PERFORMING ORGANIZATION NAME AND ADDRESS: University of Dayton Research Institute, 300 College Park Avenue, Dayton, Ohio 45469	10. PROGRAM ELEMENT, PROJECT, TASK AREA & WORK UNIT NUMBERS: Prog. Ele. 64212F, Proj. 2202, Task 220203, Work Unit 22020305
11. CONTROLLING OFFICE NAME AND ADDRESS: Flight Dynamics Laboratory (AFWAL/FIER), AF Wright Aeronautical Laboratories, AFSC, Wright-Patterson Air Force Base, OH 45433	12. REPORT DATE: August 1980
	13. NUMBER OF PAGES: 88
14. MONITORING AGENCY NAME & ADDRESS (if different from Controlling Office): 1.187	15. SECURITY CLASS. (of this report): Unclassified
	15a. DECLASSIFICATION/DOWNGRADING SCHEDULE

16. DISTRIBUTION STATEMENT (of this Report)

Approved for public release; distribution unlimited.

17. DISTRIBUTION STATEMENT (of the abstract entered in Block 20, if different from Report)

18. SUPPLEMENTARY NOTES

19. KEY WORDS (Continue on reverse side if necessary and identify by block number)

Aircraft Transparencies
Bird Load Models
Bird Impact
MAGNA
Dynamic Response Analysis

20. ABSTRACT (Continue on reverse side if necessary and identify by block number)

The objective of the program was to experimentally and analytically examine the range of applicability of existing bird loading models. The program consisted of two primary tasks; (1) the design of an experiment and the collection of experimental data for actual bird impact on a flexible target, and (2) the computation of the response to the experimental impact conditions using the MAGNA code and existing bird loading models.

DD FORM 1 JAN 73 1473 EDITION OF 1 NOV 65 IS OBSOLETE

Unclassified

SECURITY CLASSIFICATION OF THIS PAGE (When Data Entered)

20. (continued)

Projectiles made of bird simulant material were launched at specially designed aluminum targets at velocities in the range of 60 to 300 m/sec. Impacts were at angles of 90 (normal), 45, and 25 degrees for nominal bird weights of 77 and 560 grams. Time history of target out-of-plane surface displacement was measured for all impacts and strain gage data was collected for selected impacts. Calculated response data is compared to experimental data for selected impact conditions. It is demonstrated that good results can be obtained with an uncoupled loading model using a priori information to modify the loading model. The amount of a priori information required generally increases with the degree of nonlinearity in the response and the complexity of the structure. Development of a fully coupled load model for use with the MAGNA code is recommended.

FOREWORD

The effort reported herein was conducted for the Air Force Flight Dynamics Laboratory, Wright-Patterson Air Force Base, Ohio, under Contract F33615-76-C-3103, Project 2202, "Birdstrike Windshield Technology Program". Air Force administrative direction and technical support was provided by Mr. Robert E. McCarty, AFWAL/FIER.

The work described herein was conducted during the period January 3, 1978 to December 1979. Project supervision was provided by Mr. Dale H. Whitford, Supervisor, Aerospace Mechanics Division, University of Dayton Research Institute. Experimental support was provided by the Impact Physics Group of the Experimental and Applied Mechanics Division.

The authors wish to acknowledge the contributions of Mr. David P. Bauer who was responsible for the experimental studies and Dr. H. C. Rhee who conducted a portion of the analytical investigations.

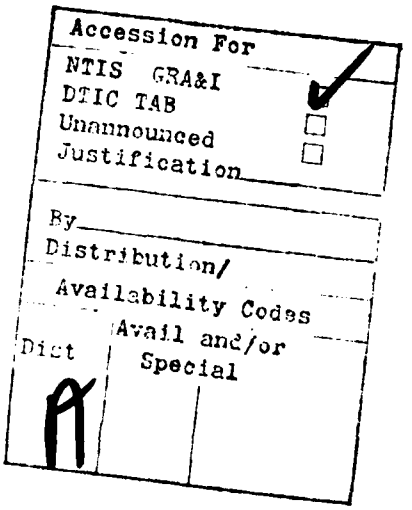

TABLE OF CONTENTS

LIST OF FIGURES

LIST OF FIGURES (continued)

LIST OF FIGURES (continued)

LIST OF TABLES

SECTION 1
INTRODUCTION

Birdstrike on aircraft has been a recognized problem since the 1940's. As a result of increased speeds of modern aircraft in low altitude missions, the potential for severe damage, loss of aircraft, and loss of life has greatly increased. Recently, the Flight Dynamics Laboratory has funded a number of birdstrike windshield technology programs to develop the technology and methodology to design and analyze aircraft transparencies and support systems.

Birdstrike protection requirements have led to the use of tough, ductile modern transparency materials such as polycarbonate and to a lessor extent stretched acrylic. This coupled with the high visibility requirements of fighter and trainer aircraft have resulted in crew enclosure structures whose response is very nonlinear during a high energy bird impact event.

Recent studies [1, 2, 3, 4, 5] conducted on rigid flat plates have shown that the bird behaves like a fluid during the impact event. For these studies the spatial and temporal distribution of the pressures during the impact event were characterized. However, during impact on a flexible target

---

[1] J. P. Barber, and J. S. Wilbeck, The Characterization of Bird Impacts on a Rigid Plate: Part I. (AFFDL-TR-75-5, ADA021142, January 1975.)

[2] J. P. Barber, H. R. Taylor, and J. S. Wilbeck, Bird Impact Forces and Pressures on Rigid and Compliant Targets. (AFFDL-TR-77-60, ADA061-313, May 1978.)

[3] A. Challita, and J. P. Barber, The Scaling of Bird Impact Loads. (AFFDL-TR-79-3042.)

[4] T. S. Wilbeck, Impact Behavior of Low Strength Projectiles. (AFML-TR-77-134, July 1978.)

[5] R. L. Peterson and J. P. Barber, The Scaling of Bird Impact Forces in Aircraft Windshield Design. (AFFDL-TR-75-150, ADA026-628, March 1976.)

(such as a polycarbonate transparency) the magnitude, duration, and distribution of the force imparted by the bird is affected by the instantaneous displacement, curvature, and velocity of the target. Thus, the load and the response are coupled and the degree of this coupling is a function of the nonlinearity of the response.

The objective of the program described in this report was to experimentally and analytically examine the range of applicability of existing bird loading models, when coupled with a nonlinear transient analysis computer program. Specifically, the applicability of these predictive models to the dynamic response of crew enclosures to bird impact was examined as a function of the degree of nonlinearity exhibited by the response.

The nonlinear structural analysis computer program used in this study was the MAGNA finite element program[6] (i.e., Materially And Geometrically Nonlinear Analysis). Basically, two levels of loading models were examined; uncoupled and coupled. The uncoupled loading model was based on simple hydrodynamic theory and momentum calculations of an impact event. A complete description of the loading derived by this method can be hand calculated and entered as input data. The coupled loading model is a dynamic model in that the predicted impact loads for a given solution time step depend upon the prior response of the target. As a result the coupled loading model may be expected to produce more accurate predictions of actual transparency response due to bird impact.

The program consisted of two primary tasks; (1) the design of an experiment and the collection of experimental data for actual bird impact on a flexible target, and (2) the computation of the response to the experimental impact conditions using the MAGNA code and the existing bird load models. The calculated and experimental results were then compared and evaluated.

---

[6] R. A. Brockman, MAGNA: A Finite Element Program for the Materially and Geometrically Nonlinear Analysis of Three-Dimensional Structures Subjected to Static and Transient Loading. (UDR-TR-79-45, October 1979.)

SECTION 2
EXPERIMENTAL INVESTIGATIONS

Projectiles made of bird simulant material were launched at specially designed aluminum targets at velocities in the range of 60 to 300 m/sec. Impacts were at angles of 90 (normal), 45, and 25 degrees for nominal bird weights of 77 and 560 grams. Time history of target out-of-plane surface displacement was measured on all impacts and strain gage data was collected for selected impacts. The experimental data collected on this program is summarized herein.

Target description, instrumentation, experimental procedures, and the experimental results are discussed in the following paragraphs.

2.1 TARGET DESCRIPTION

The design of the target was influenced by the program objective, the capability of the MAGNA program, and the availability of the material characterization data required for the computer analysis. In order to represent the large overall and local deformations experienced during bird impact on flight hardware it was desirable to design a target that would undergo such deformation without experiencing failure. A second requirement was to design the target so that it could be conveniently and accurately modeled using the elements available with the MAGNA program. A logical material choice might appear to be polycarbonate since this material is tough, ductile, and is used for modern aircraft transparencies. However, the material properties for this material are not characterized with the same level of confidence as are most metals.

An additional consideration was that the stiffness of the support structure relative to the stiffness of the panel be somewhat representative of that occurring in typical flight

systems. Data from the F-111 bird resistant transparency system[7] was used as a basis for meeting this requirement.

Consideration of these design requirements together with fabrication requirements and cost resulted in the target design shown in Figures 1 and 2. Special features which were advantageous are: (1) 6061-T6 grade aluminum has well characterized material properties at all strain rates; (2) the simple geometry permitted accurate modeling and repeatable testing; (3) welding construction provided modeling advantages, less expensive fabrication, and eliminated possibilities of bolt hole tear-out and fastener failure, and; (4) the split edge stiffeners minimized the effects of welding stresses and panel "oil canning".

The targets were attached to the holding fixture through spherical bearing mounts as shown in Figures 1 and 2. This mounting technique allowed target rotation at the attachment point, thereby permitting increased flexibility for larger elastic strains. The spherical bearings were mounted to permit maximum rotation (approximately 22 degrees). No experiment caused full use of this total rotational capability.

The target mounting fixtures were especially designed for these experiments. These fixtures, rigidly constructed of heavy steel members are depicted in Figure 3. The primary instrumentation for all experiments measured target deflection with a resolution of 1 mm. Design objectives for the mounting fixture included the prevention of target rigid body motion greater than the instrumentation resolution. Tests during a worst case impact showed that the design criteria was met based on results from the moire fringe instrumentation.

---

[7] B. S. West, Design and Testing of F-111 Bird Resistant Windshield/Support Structure, Volume 1 - Design and Verification Testing. (AFFDL-TR-76-101, October 1976.)

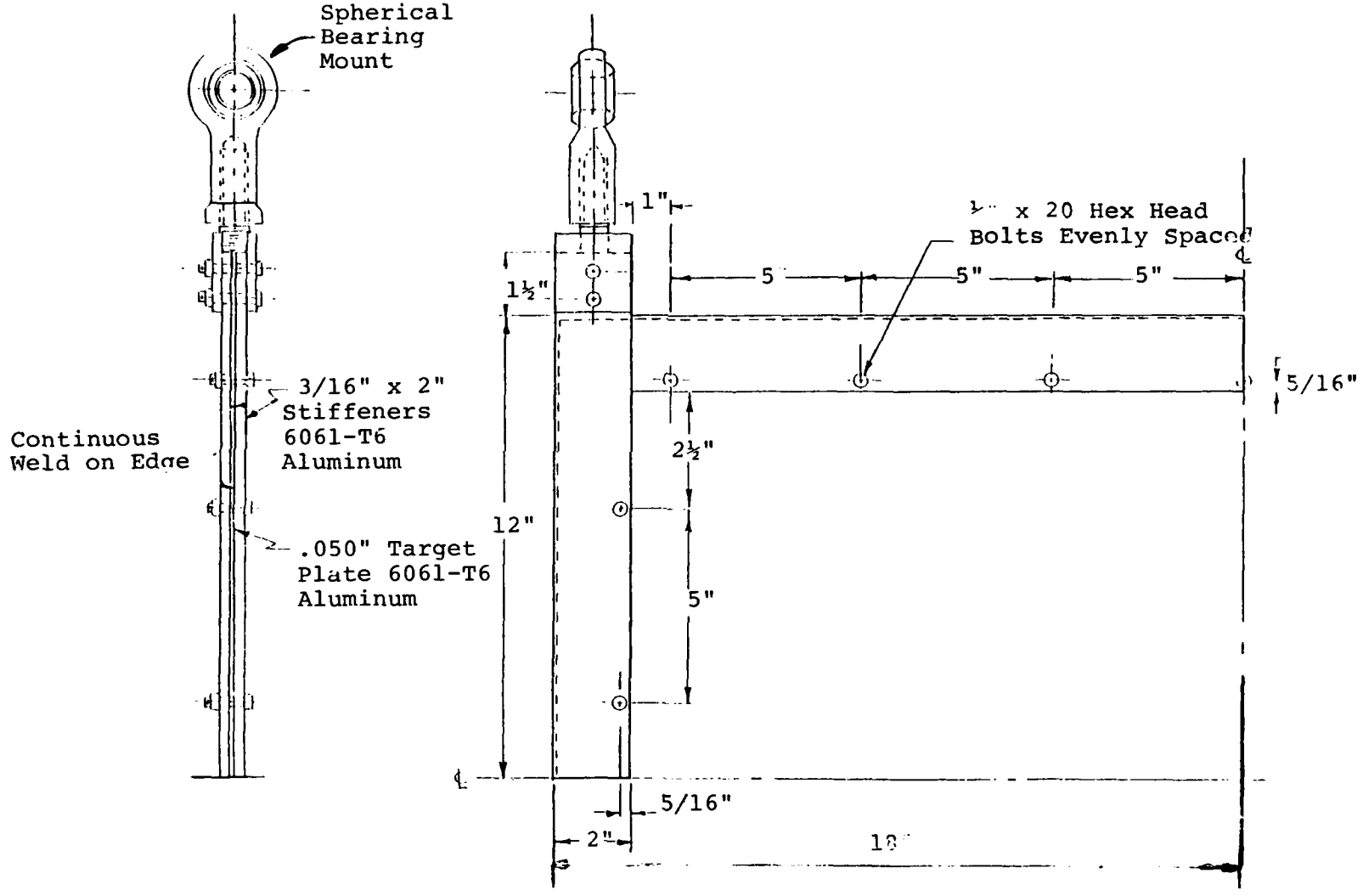

Figure 1. Sandwiched Stiffener Target Plate [¼ Plate Shown].

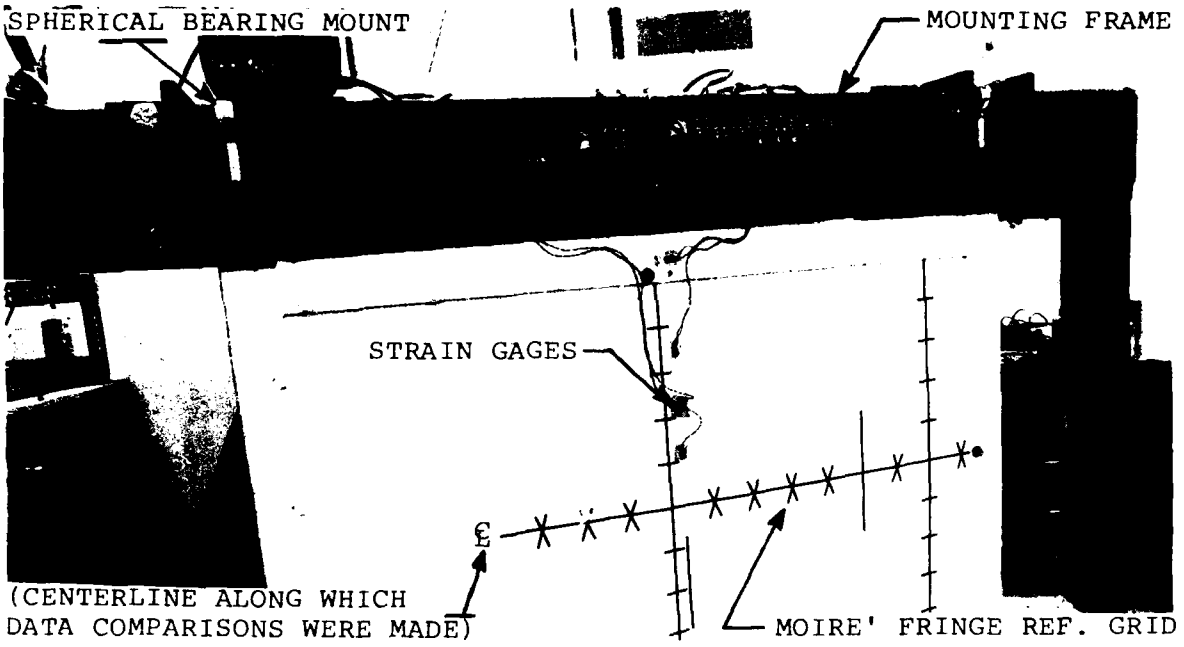

Figure 2. Photograph of Installed Target.

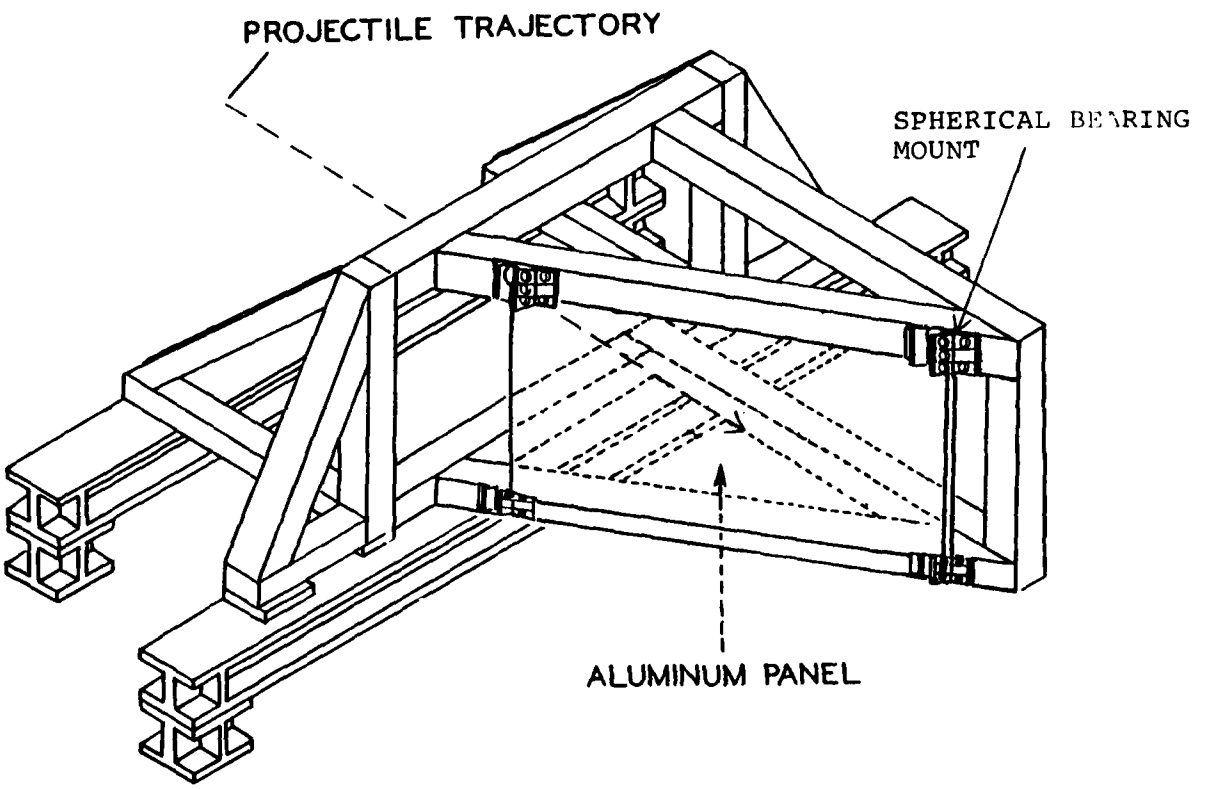

Figure 3. Support Structure and Mounting Frame.

2.2 INSTRUMENTATION

2.2.1 Projectile Velocity, Location, and Orientation Measurement

The velocity of the projectile was measured prior to impact using a simple time-of-flight technique. Between the muzzle of the sabot stripper and the target, two helium/neon laser beams were directed across the trajectory. When the projectile interrupted the first laser beam, a counter was started. The counter was stopped when the projectile interrupted the second laser beam. The distance between the laser beams and the elapsed time were used to calculate the velocity. To independently verify the velocity measurements and to determine projectile location, orientation, and integrity just prior to impact, an orthogonal x-radiographic set-up was used at each laser beam station. The first velocity station was located approximately 165.1 cm in front of the target, and the second station was located 104.1 cm in front of the target. A fiducial system was located in each field of view to provide a reference system by which location measurements could be made. A typical record of a projectile in flight from one of these stations is shown in Figure 4. Measurements were made on records like that shown in Figure 4 to find projectile location and orientation prior to impact. The pitch and yaw of the projectile could be determined by using the orthogonal sets of x-radiographs provided by the system. Projectile location could be measured to within about 1.25 mm providing a velocity accuracy of about one percent. Orientation could be measured to within ± 0.5°.

2.2.2 Target Displacement Measurement

Projectile impact on the target resulted in out-of-plane displacement which varied as a function of the impact velocity and bird mass. The primary target instrumentation recorded this displacement motion for each shot by using an experimental technique based on the moire' fringe light interference

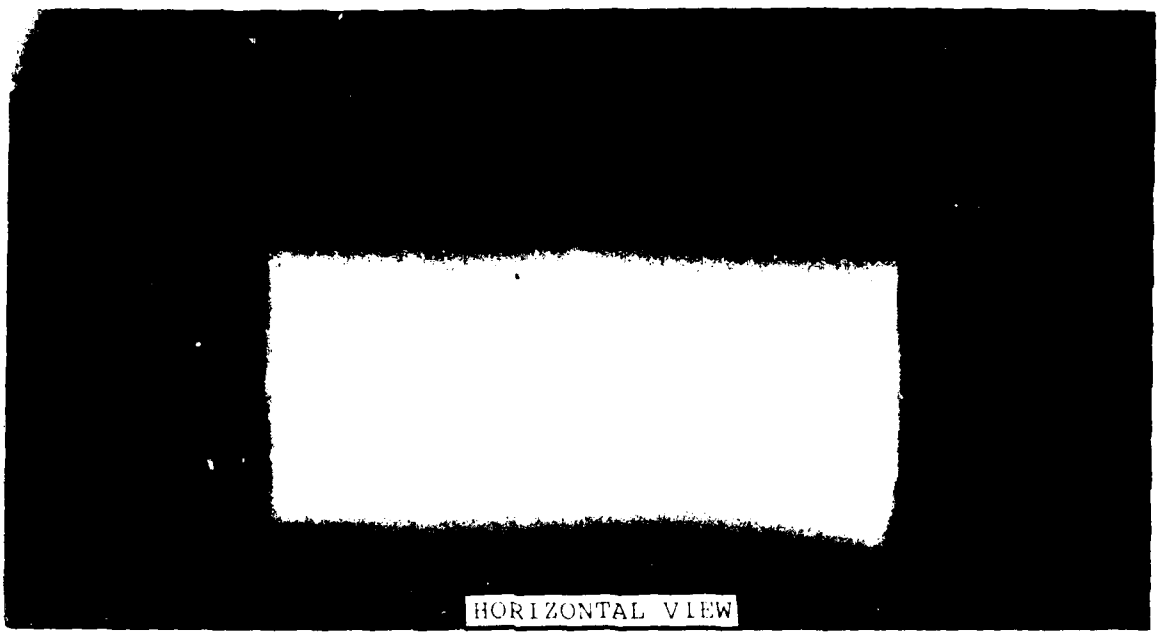

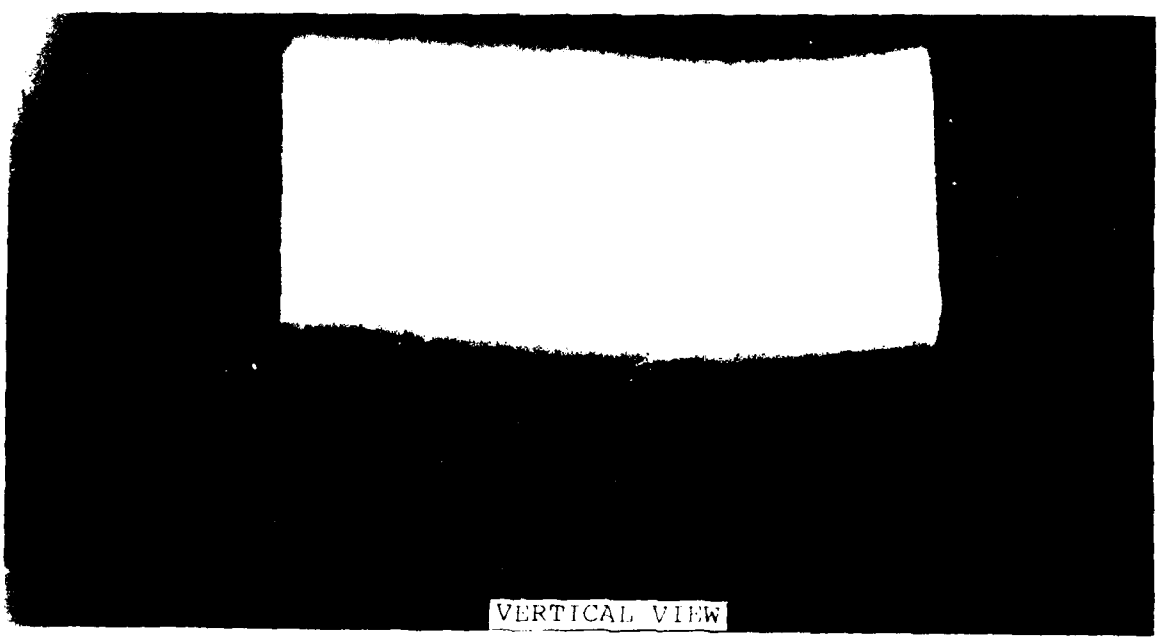

Figure 4. Projectile in Flight.

principle. The basic experimental technique and the device itself are fully described in Reference 8. Figures 5 and 6 show the device. The technique features a non-contacting displacement measurement over a field-of-view area about 43 cm in diameter. The resolution of the system was about 1 mm. Data were recorded from the moire' fringe device by a high speed framing camera onto 16 mm film. Film speed through the camera was about 6,500 frames per second giving a time resolution of 150 microseconds. The light source used with the system allowed recording of data for about 15 milliseconds. Only the data required to accurately characterize the panel displacement were reduced from the large quantity recorded by the experimental set-up. Usually the early time displacements along a symmetry axis provided adequate information and these results are shown in the following sections. A typical sequence of moire' fringe patterns as a function of time is shown in Figure 7.

2.2.3 Strain Measurement

Strain data were collected on several selected shots. Strain gages were mounted on both sides of the targets as shown in Figure 8. Standard temperature compensated gages and mounting techniques were used to attach the gages. Strain bridges with 80 KHz frequency response capabilities were used with the strain gages in completion circuits. The strain data were recorded digitally on a 200 KHz bandwidth electronic recorder. This recorder allowed a total recording time of about 10 milliseconds.

2.3 EXPERIMENTAL PROCEDURES

Obtaining desired target displacement during an experimental birdstrike event requires that projectiles be launched at controlled velocities. This section contains a brief description of the launch techniques used at the UDRI

---

[8] Andrew J. Piekutowski, A Device to Determine the Out-of-Plane Displacement of a Surface Using a Moire' Fringe Technique. (UDR-TR-79-58 6 May 1979.)

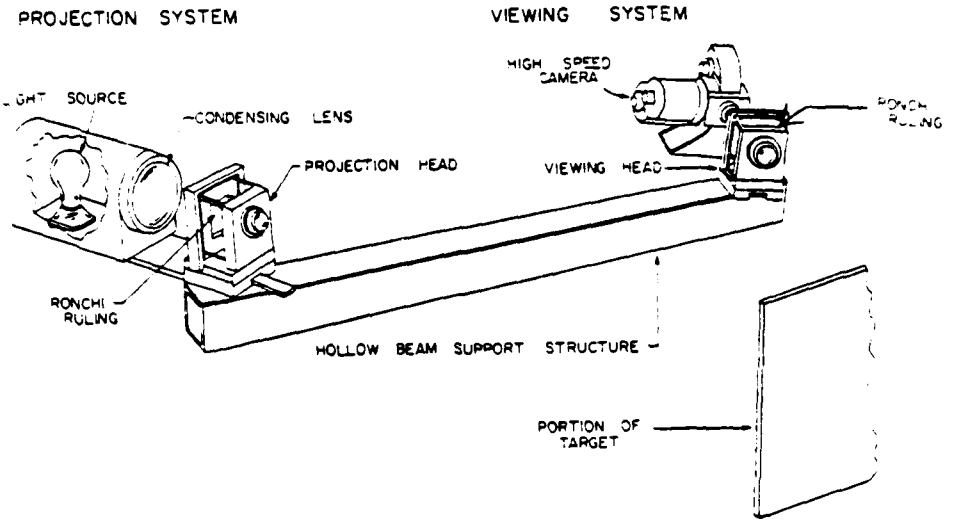

Figure 5. Schematic View of Moire' Device Illustrating Components and their Relationship to Target Surface.

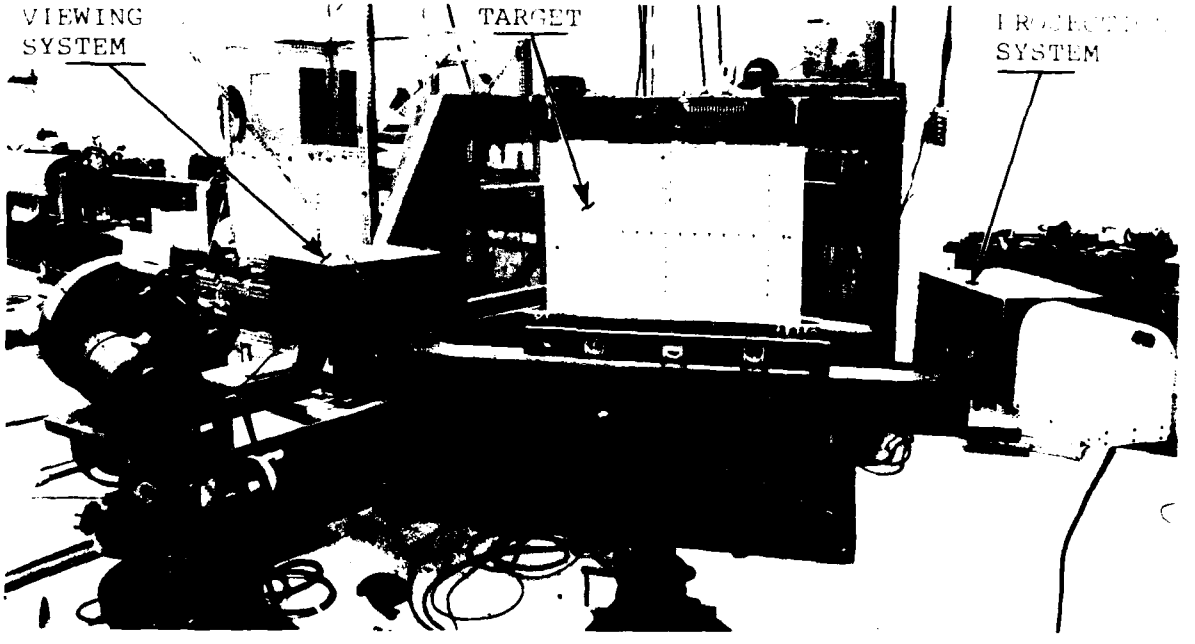

Figure 6. Typical Test Set-Up Showing Moire' Fringe Device. (Looking up Range).

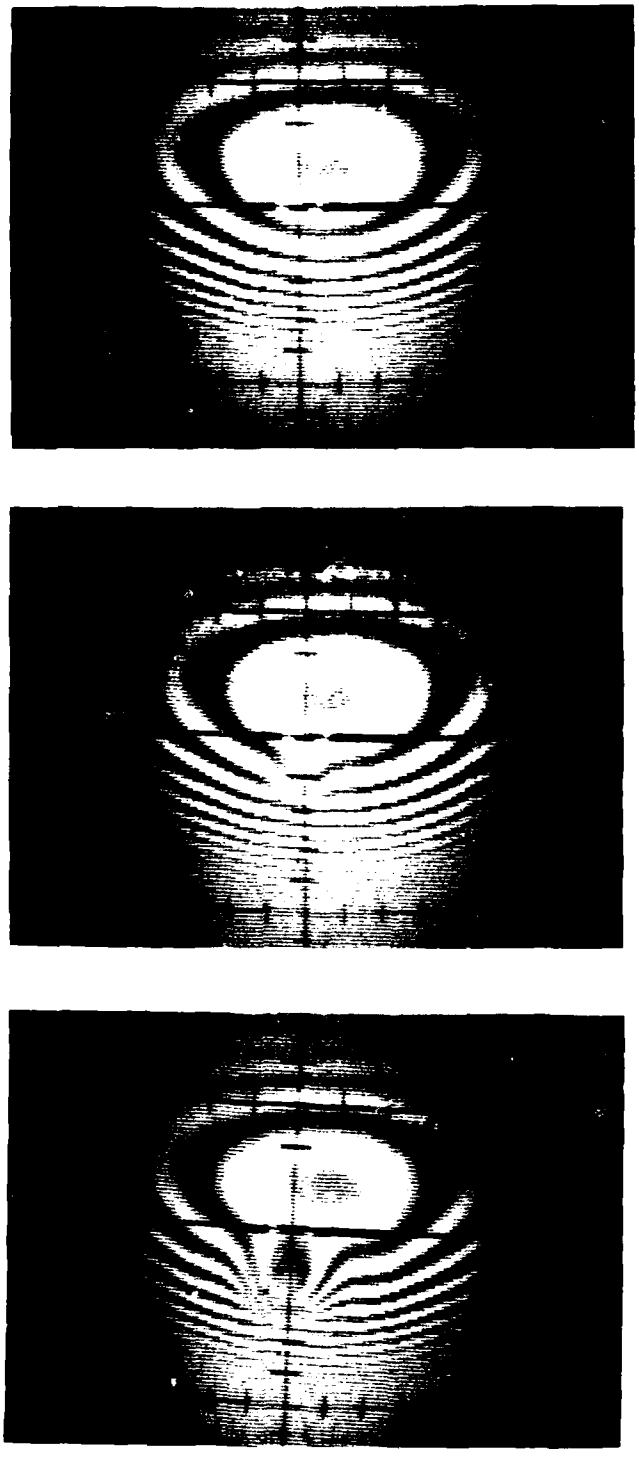

Figure 7. Typical Sequence of Moire' Fringe Patterns with Increasing Time.

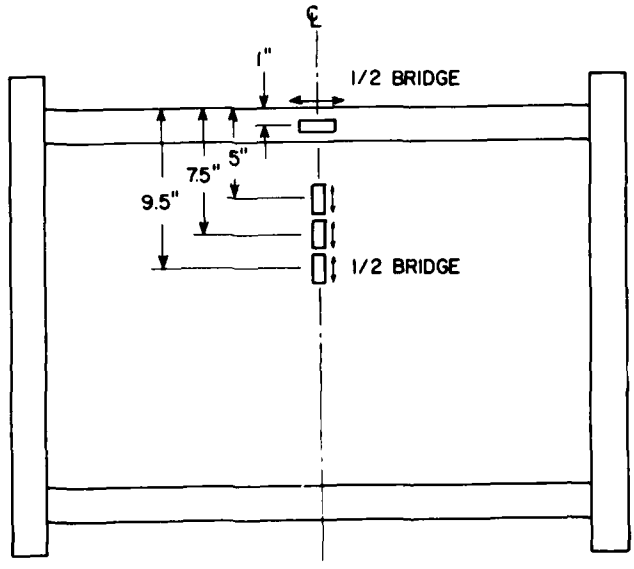

Figure 8. Strain Gage Locations.

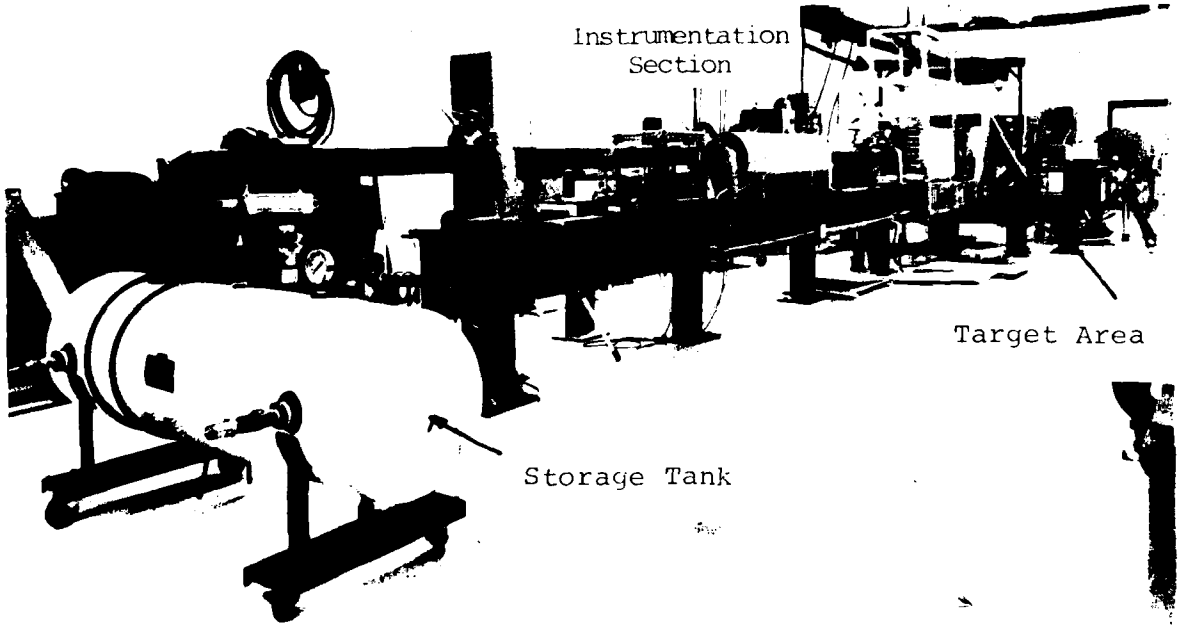

Figure 9. Overall View of the 88.9 mm Gun Range.

facilities. Figure 9 shows an overall view of the range as it was assembled for these tests.

A compressed gas gun was used to accelerate the projectiles. The launch tube for the gun was an 88.9 mm ID, 3.66 m long steel tube. Compressed air stored in a $0.32 m^3$ steel tank was used as the propellant. The air pressure inside the tank was adjusted to control projectile velocity from 50 m/s to 300 m/s. Maximum driving pressure was 2.07 MN/m^2. The compressed air was transferred from the tank to the rear of the projectile package via an 88.9 mm diameter pneumatically operated butterfly valve.

The projectile was placed in a geometrically compatible pocket of an 88.9 mm OD foamed polyurethane sabot, as shown in Figure 10. The projectiles were right circular cylinders made of gelatin and phenolic microballoon. This material has been well characterized and was used to closely simulate the behavior of real birds. References 4 and 9 characterize in detail the impact behavior of the microballoon gelatin as compared to real birds. In an effort to adequately explore the range of target response, two projectile sizes were employed.

A small projectile 3.81 cm in diameter by 7.62 cm long and a large projectile of 7.62 cm diameter by 15.24 cm long were used. The microballoon gelatin material was used at a density of 0.92 g/cm^3, resulting in nominal projectile masses of 77 g and 560 g respectively. The simulant material consisted of 77 percent, by weight of water, 19 percent industrial bloom type A gelatin, and 4 percent phenolic microballoon.

The sabot carrying the projectile was not allowed to strike the target. A reduced ID section of steel tube

---

[4] T. S. Wilbeck, Impact Behavior of Low Strength Projectiles. (AFML-TR-77-134, July 1978.)

[9] David P. Bauer, and John P. Barber, Experimental Investigation of Impact Pressures Cased by Gelatin Simulated Birds and Ice. (UDR-TR-78-114, March 1979.)

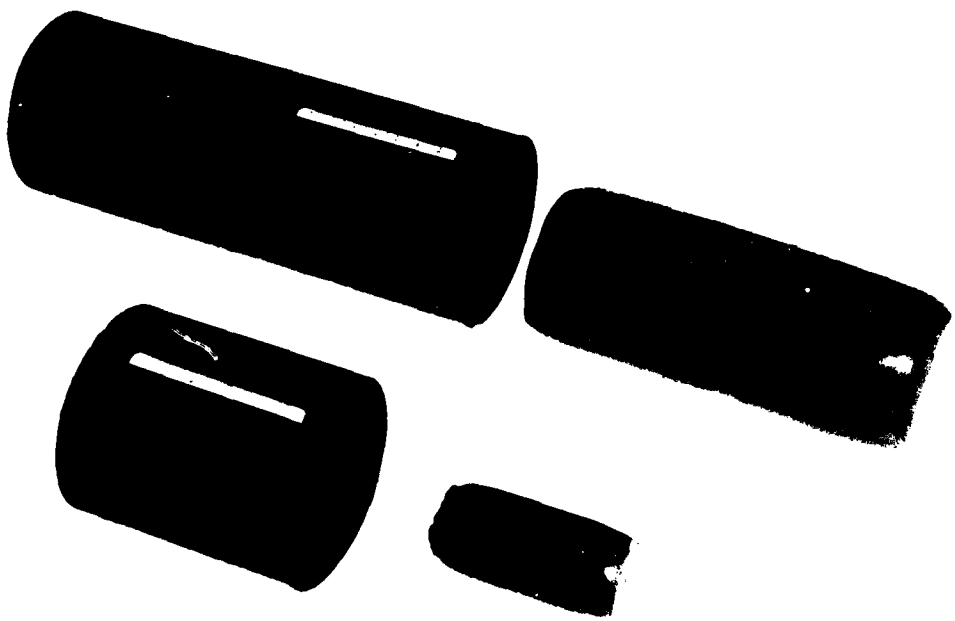

Figure 10. Photograph of Typical Artificial Bird and Foam Plastic Sabot.

connected to the launch tube muzzle was used to stop the sabot. The projectile sabot package entered the tapered section of tube slowing the sabot to a stop while allowing the projectile to continue unimpeded to the target. The stopped sabot also served to deflect the high velocity propellant gas laterally away from the projectile trajectory through slots in the stripper tube. This technique prevented the propellant gas from impinging on the target.

2.4 EXPERIMENTAL RESULTS

The 46 experimental shots made during this program are summarized in Table 1. Approximately 12 additional developmental shots were made.

TABLE 1

SUMMARY OF EXPERIMENTAL RESULTS

ANGLE	SHOT NUMBER	MASS g	VELOCITY m/sec	LOCATION	DATA	COMMENT
25°	40139	82.0	200	center	moire/st. gauges	useable film/strain data recorded
25°	40117	73.9	129	center	moire	useable film
25°	40115	72.9	133	center	moire	useable film
25°	40122	84.3	233	center	hycam	color film bird flow-impact side
25°	40121	84.3	243	center	moire	useable film
25°	40119	84.1	294	center	moire	useable film
25°	40116	75.5	294	center	moire	useable film
25°	40130	86.4	200	center low	moire	unuseable film
25°	40124	83.2	230	rt. center	moire	useable film
25°	40129	86.6	180	rt. corner	moire	useable film
25°	40127	86.9	261	rt. corner	moire	useable film
25°	40118	571.3	101	center	moire	unuseable film
25°	40123	559.3	130	center	moire	useable film
25°	40120	559.1	154	center	moire	useable film
25°	40126	559.3	158	rt. center	moire	useable film
25°	40125	559.0	160	rt. center	moire	unuseable film
45°	40140	86.0	204	center	moire/st. gauges	useable film/strain data recorded
45°	40094	74.6	163	center	moire/st. gauges	useable film/no strain data
45°	40092	76.7	99	center	moire	useable film
45°	40082	78.2	237	center	moire	useable film
45°	40083	80.1	257	center	moire	useable film
45°	40133	90.2	175	rt. center	moire	useable film
45°	40089	78.2	195	rt. center	moire	unuseable film
45°	40090	76.6	195	rt. center	fastax	configuration test, useable film
45°	40088	76.2	274	rt. center	moire	unuseable film
45°	40131	86.0	177	center low	moire	useable film
45°	40132	88.5	176	rt. corner	moire	useable film
45°	40087	560.1	105	center	moire	useable film
45°	40086	568.2	133	center	moire	useable film
45°	40085	557.8	159	center	moire	useable film
90°	40049	84.7	155	center	moire/st. gauges	useable film/strain data recorded
90°	40048	599.1	64	center	moire/st. gauges	useable film/strain data recorded
90°	40138	86.2	72	center	moire	useable film
90°	40135	87.3	74	center	moire	unuseable film
90°	40029	83.8	159	center	moire	useable film
90°	40031	84.1	195	center	moire	useable film
90°	40044	84.0	198	center	moire	useable film
90°	40045	82.2	237	center	moire	useable film
90°	40078	85.3	238	center	moire	useable film
90°	40047	82.2	240	center	moire	useable film, panel failed
90°	40046	83.0	280	center	moire	useable film
90°	40134	90.0	129	rt. center	moire	useable film
90°	40136	89.5	120	center low	moire	useable film
90°	40137	86.5	119	rt. corner	moire	useable film
90°	40051	579.8	101	center	moire	useable film
90°	40050	573.6	102	center	moire	useable film

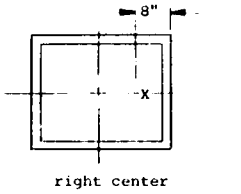

right center

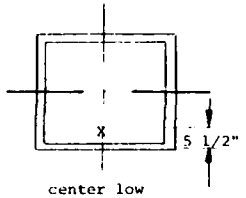

center low

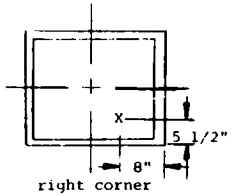

right corner

SECTION 3
ANALYTICAL INVESTIGATIONS

3.1 BIRD LOADING MODELS

The descriptions of structural loading due to bird impact which are discussed herein are of two types. The first is an uncoupled model, which does not account for local deformation of the target during impact. This rather simplistic representation of soft-body impact loading is considered in order to identify problem characteristics (such as severity of impact or extent of deformation) which may determine the range of applicability of simplified loading models. Secondly, a coupled loading model is considered, which attempts to predict the impact pressure distribution at distinct points in time based upon the current deformed geometry of the target surface. Study of the coupled impact loading model is intended to define the range of problem parameters for which it may be used with confidence, and to determine possible areas for future improvement.

3.1.1 Uncoupled Loads Model

Although a certain dependence of bird impact loading upon the local structural response of the target surface is known to exist, a simplified representation of the dynamic loading appears quite attractive in many instances. For example, windshield enclosures made of relatively brittle materials (e.g., tempered glass and stretched acrylics) exhibit only small to moderate deformations prior to catastrophic failure, and the effects of load-response coupling in this case is presumably small. While the only true justification for using an uncoupled loading description is the reduction in computing time, the savings over a detailed, coupled model could be considerable. Thus, it is appropriate to study this class of loads models to determine its suitability for impact simulation in which the influence of coupling is expected to be minor.

The particular uncoupled loading model employed in the present study is due to Barber, Taylor and Wilbeck.[2] This model is based upon a simple transfer of momentum analysis, with the following assumptions:

- the target is completely rigid,
- the bird behaves as a fluid during impact,
- the component of bird momentum normal to the target is transferred completely to the target, and
- no deceleration of the bird occurs during impact.

For the purpose of computing impact duration and loaded area, the shape of the bird is idealized as a circular cylinder whose length is twice its diameter. Details of the uncoupled loading model may be found in Reference 2; however, a summary of the pertinent equations is given below for completeness.

For perfect momentum transfer from the bird to the target, the total (normal) impulse is

$$I = mv \sin\theta \tag{3.1}$$

where, m,v are the bird mass and velocity, and θ is the angle of impact, with $\theta=90°$ corresponding to normal impact. The time interval over which the impact occurs is estimated from

$$T = \ell_{eff}/v, \tag{3.2}$$

in which ℓ_{eff} is an "effective length"

$$\ell_{eff} = \ell + \frac{d}{\tan\theta}. \tag{3.3}$$

---

[2] J. P. Barber, H. R. Taylor, and J. S. Wilbeck, Bird Impact Forces and Pressures on Rigid and Compliant Targets. (AFFDL-TR-77-60, ADA061-313, May 1978.)

This definition of the effective length is useful in oblique impact situations (see Figure 11). From Equations 3.1 and 3.2, it is possible to compute the average normal force during impact,

$$F_{avg} = mv^2 \sin\theta/\ell_{eff}. \qquad (3.4)$$

The simplest representation of total impact force versus time is obtained by applying the estimated average force (Equation 3.4) over the entire interval $0<t\leq T$; this particular loading variation is referred to subsequently as a "square pulse" load. Experimental data summarized in Reference 2 indicate that the actual peak force is approximately twice F_{avg}, and that this peak force occurs roughly at $t/T = 0.2$. A force-time profile which reflects these observations is the "triangular pulse",

$$F(t) = \begin{cases} 10\ F_{avg}\ (\frac{t}{T}) & ;\quad 0\leq t\leq 0.2T \\ \\ \frac{5}{2}\ F_{avg}\ (1-\frac{t}{T}) & ;\quad 0.2T\leq t\leq T. \end{cases} \qquad (3.5)$$

Both of these force-time signatures (shown in Figure 12) are used in the present study.

The above model yields information concerning the time interval and total force associated with impact loading, but does not consider the spatial distribution of loading on the target.

For normal impacts, the assumed pressure distribution used here consists of a constant pressure applied over a circular area with radius equal to that of the bird. Some computations have also been performed using a constant pressure on an area whose radius is twice that of the bird,

---

[2] J. P. Barber, H. R. Taylor, and J. S. Wilbeck, Bird Impact Forces and Pressures on Rigid and Compliant Targets. (AFFDL-TR-77-60, ADA061-313, May 1978.)

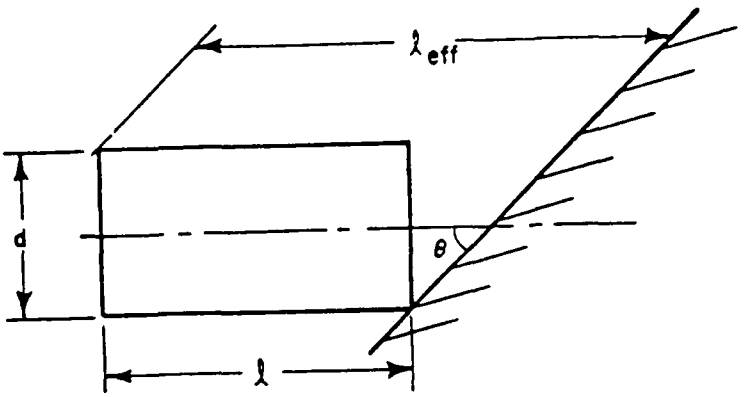

Figure 11. Oblique Impact Geometry and Definition of Effective Length.

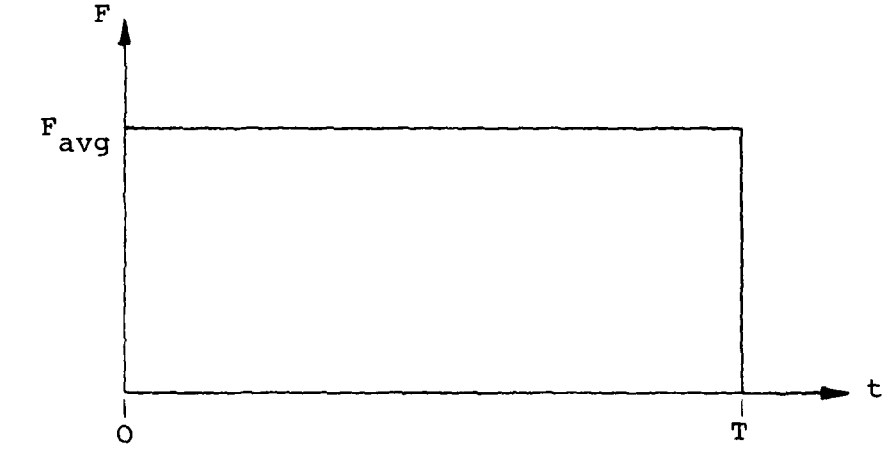

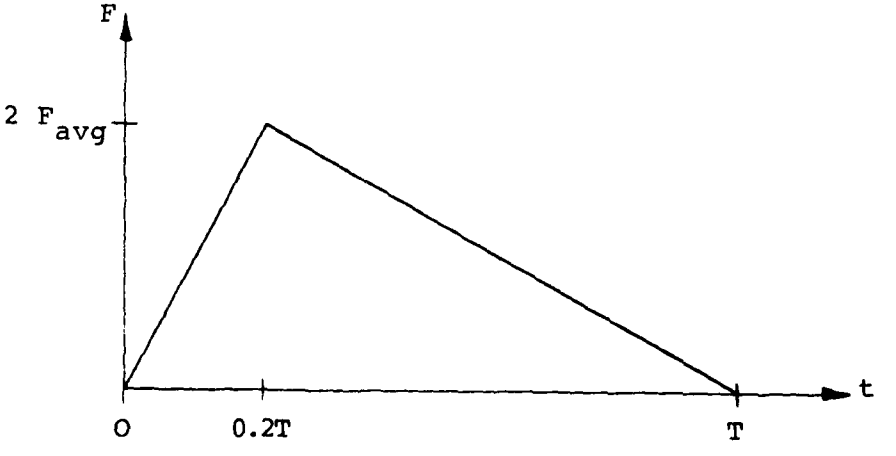

Figure 12. Square and Triangular Pulse Loading.

as a means of accounting for spreading out of the loaded areas as the impact proceeds.

For oblique impacts, the spatial distribution and loaded area are based on the steady flow pressure distributions presented in Figures 34 and 35 of Reference 2*. These spatial pressure distributions were idealized as shown in Figures 13 and 14 for both 45 and 25 degree impacts. An elliptical loaded area defined by the projection of the cylindrical bird on the oblique surface was used. This area is defined mathematically by the expression

$$\frac{x^2}{(a/\sin\theta)^2} + \frac{y^2}{a^2} = 1 \qquad (3.6)$$

where a is the bird radius, $a/\sin\theta$ is the intercept on the major axis, and a is the intercept on the minor axis. The temporal distribution of the load was a triangular pulse as depicted in Figure 12 and the load F(t) at any time t is found by integrating the idealized pressure distribution over the area of the ellipse defined by Equation 3.6.

3.1.2 Coupled Loads Model

A loading model which includes the effects of coupling between impact pressures and local surface deformations has also been considered during the present study. The model, based on the methodology of Reference 2, is based upon the superposition of linear potential flow solutions for steady flow in a circular duct and for a uniform distribution of source elements on an elliptical surface.

---

[2] J. P. Barber, H. R. Taylor, and J. S. Wilbeck, Bird Impact Forces and Pressures on Rigid and Compliant Targets. (AFFDL-TR-77-60, ADA061-313, May 1978.)

---

*It should be emphasized that, although the loaded area and the spatial loading distribution are both time-dependent, the steady flow solution of Reference 2 does not reflect this dependence. This lack of information concerning the time variation of the loading is considered to be a serious deficiency in the loading model of Reference 2.

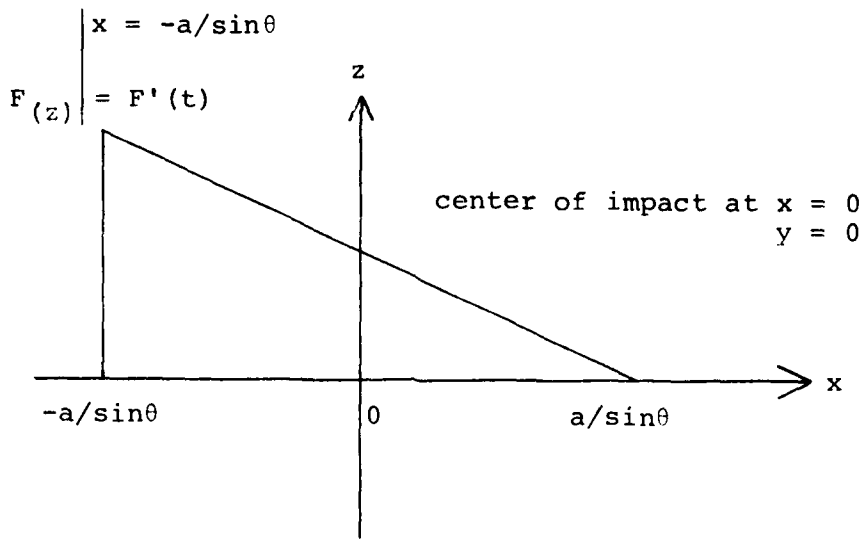

Figure 13. Idealized Pressure Distribution Along Major Loading Axis for Oblique Impact Load Model.

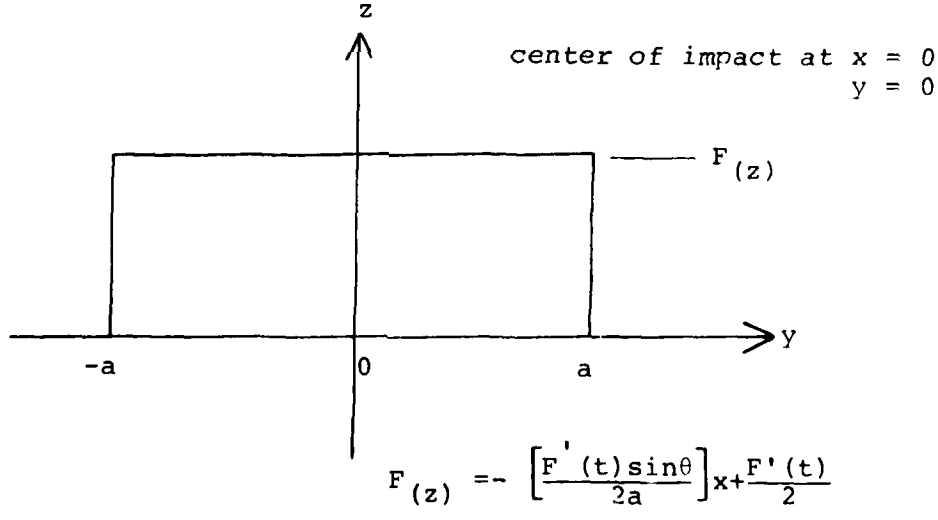

Figure 14. Idealized Pressure Distribution Along Minor Loading Axis for Oblique Impact Loading Model.

Attempts to implement this loading model within the finite element structural analysis program have not been successful. Despite considerable modification to the original loads analysis program to reduce storage to a workable level, take advantage of symmetry, and account for different levels of mesh detail in the structural and loading data, acceptable results have not been obtained.

Apparently, the coupled model has difficulty in resolving the flow boundary conditions correctly, since the analysis produced rather large negative pressures on the periphery of the impact region in normal impact problems. Oblique impact cases, which are analyzed differently by the loads program, could not be executed successfully.

The coupled model of Reference 2 appears to be somewhat inappropriate for the analysis of general three-dimensional impacts on windshield-type structures, since the formulative basis of the model is lacking in generality. The windshield impact problem can involve quite arbitrary geometry, as well as very large local rotations, and a general formulation of the problem for finite element or finite difference solution seems preferable. The loading model of Reference 2 appears to be more appropriate for the analysis of soft-body impacts on blades or similar components, for which the localized deformations are less severe and the flow boundary conditions affect the surface pressure field to a lesser extent[10].

3.2 STRUCTURAL SIMULATION

All of the numerical analyses conducted during the present study were performed using the nonlinear finite element program

---

[2] J. P. Barber, H. R. Taylor, and J. S. Wilbeck, Bird Impact Forces and Pressures on Rigid and Compliant Targets. (AFFDL-TR-77-60, ADA061-313, May 1978.)

[10] L. I. Boehman, and A. Challita, Model for Predicting Bird and Ice Impact on Structures. (UDR-TR-79-54, February 1980.)

MAGNA (Materially And Geometrically Nonlinear Analysis)[6]. The following sections provide a brief description of the finite element modeling procedures.

3.2.1 Structural Models

Two different finite element models (Figure 15) of the experimental target plate have been employed in the numerical investigations. For normal impacts, a doubly symmetric model of one quadrant of the plate is used, while oblique impact angles permit the use of only one plane of symmetry.

Since the primary means of evaluating the accuracy of the computations is by comparison of predicted deflections with experimental data, the models have been constructed only in sufficient detail to provide reasonably smooth deflection data. It is noted that a considerably finer mesh would be needed in both cases to obtain detailed information concerning local stress fields near the impact site.

Information concerning the size of each of the finite element models is given in Table 2. Both models are fully three-dimensional, using the twenty-node version of the variable-number-of-nodes solid element in MAGNA. Full geometrical (large-displacement) and material (plasticity) nonlinearities are included. The nonlinear dynamic equations have been solved using Newmark's method of integration, with tangent stiffness matrices being recomputed and solved at every time step.

The target plate material (6061-T6 aluminum) is represented by the properties listed in Table 3. Values of stress versus plastic strain which appear in the table serve

---

[6]R. A. Brockman, MAGNA: A Finite Element Program for the Materially and Geometrically Nonlinear Analysis of Three-Dimensional Structures Subjected to Static and Transient Loading. (UDR-TR-79-45, October 1979.)

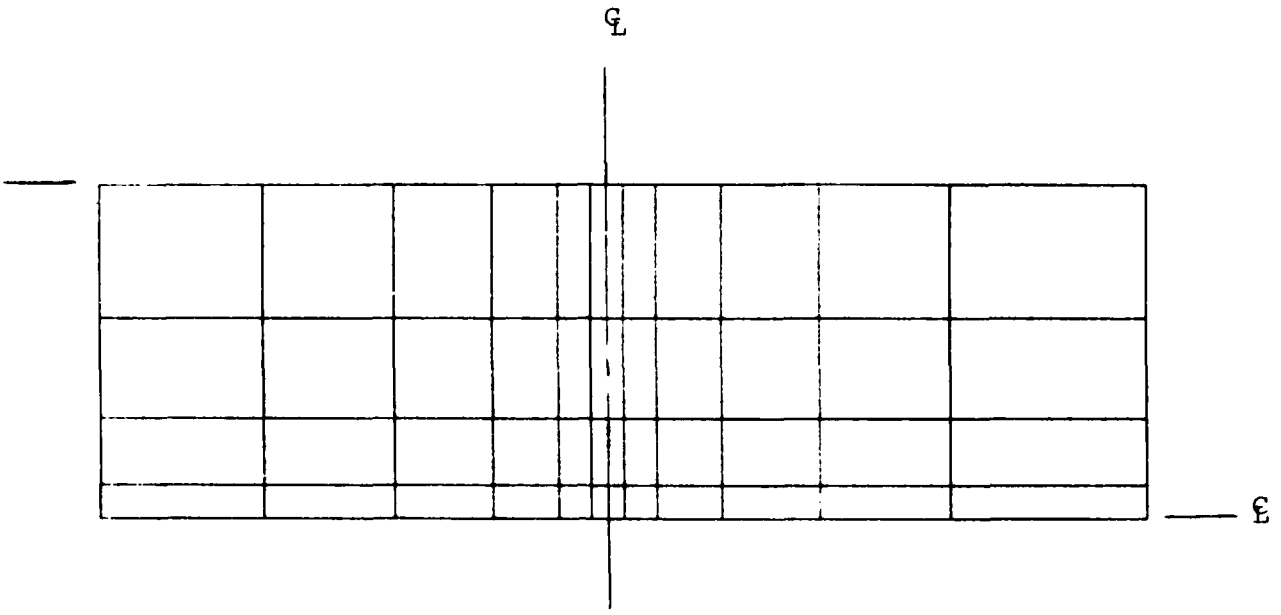

Half Plate Model

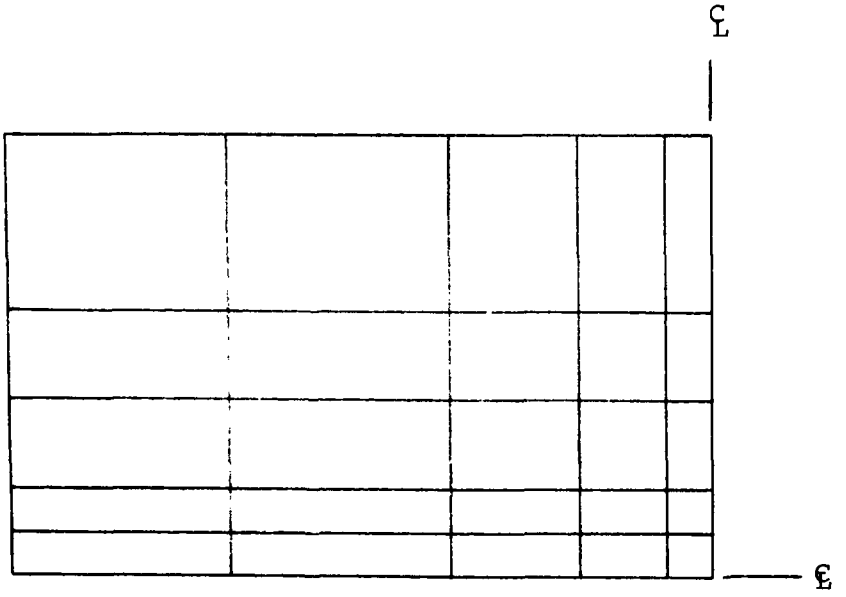

Quarter Plate Model

Figure 15. Finite Element Models.

TABLE 2

FINITE ELEMENT MODEL STATISTICS

	Quarter-Plate	Half-Plate
Node Points	228	386
Elements	25	44
Nodes/Element	20	20
Degrees of Freedom	475	818

TABLE 3

MATERIAL PROPERTIES FOR ALUMINUM 6061-T6

Elastic Modulus	$E = 1.0 \times 10^7$ p.s.i.
Poisson's Ratio	$\nu = 0.330$
Mass Density	$\rho = 0.00025362$ lbf-sec.^{2}/in.^{4}
Yield Stress	$\sigma_y = 34878.$ p.s.i.

Stress Versus Plastic Strain Curve:

ε_p	σ
0.	34878.
0.000253	37351.
0.001062	39303.
0.002021	39761.
0.057532	42453.
1.	42453.

to define the piecewise linear stress-strain curve in the elastic-plastic range; for plastic strains greater than 0.057532 in./in., the material assumed to be perfectly plastic. Isotropic strain hardening has been used in all cases. It should be noted that the elastic-plastic analysis performed by MAGNA uses a subincremental technique to reduce the accumulated errors. In all of the analyses reported herein, a strain increment limit of 0.0002 has been imposed; that is, the constitutive relations are reevaluated at a sampling point whenever any incremental component of strain reaches 0.02 percent.

3.2.2 Loading Models

The representation of loading in the finite element simulations results from a consistent application of the finite element displacement approximation to the surface load distributions obtained in Section 3.1. In particular, the virtual work of impact forces on the flat plate is

$$\delta W_e = \int_A p(x,y)\ \delta w\ dA \tag{3.7}$$

where x,y are coordinates within the surface and w is the transverse displacement. For a finite element in which

$$w \approx \underset{\sim}{W}^T \underset{\sim}{N}, \tag{3.8}$$

$\underset{\sim}{N}$ being the shape functions, the consistent loads are

$$\underset{\sim}{P} = \int p(x,y)\underset{\sim}{N}\ dA. \tag{3.9}$$

In the present situation, evaluation of Equation 3.8 must be performed by a specialized method which permits pressure discontinuities within individual elements. The loaded area is circular or elliptical, while the finite element mesh is rectangular, as shown in Figure 16. A special purpose preprocessing program has been used to evaluate the consistent loads vector $\underset{\sim}{P}$ by the simple summation formula

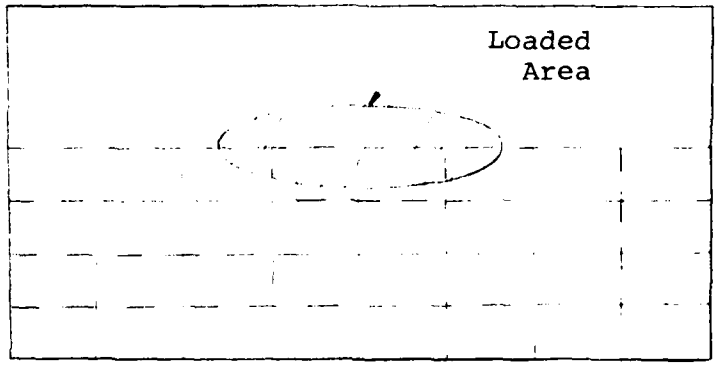

Loaded Area of
Finite Element Mesh

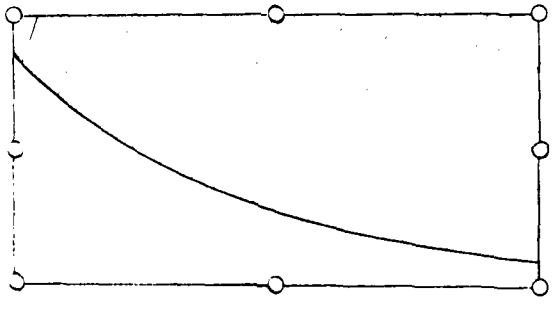

Partially-Loaded
Element

Figure 16. Loading on Finite Element Model Surface.

$$\underset{\sim}{P} = \sum_{i-1}^{m} \sum_{j=1}^{n} p(x_i, y_j) \underset{\sim}{N} \Delta x \Delta y \qquad (3.10)$$

in which $\Delta x = x_{i+1} - x_i$, etc. In each loading case, m and n have been made sufficiently large to obtain converged values for $\underset{\sim}{P}$ (typically, $m = n \approx 100$, for partially loaded elements).

3.3 ANALYTICAL PROCEDURES

Because of the large computer run times associated with nonlinear dynamic solutions a tentative computer run matrix was identified which would address the program objective in an efficient manner. This matrix is presented in Table 4. Examination of this table reveals that the problem was to be investigated with respect to impact angle, impacting energy level, load model, loaded area, and bird size. Individual points in this tentative matrix were given priority and the entire matrix was evaluated in terms of the results obtained on a continuous basis. Therefore, not all points were actually computed. A matrix of the conditions for which solutions were obtained is presented in Table 5. One impact condition (shot No. 40048) was also run. However, the results indicated that the finite element model used for the small bird impacts was not adequate for the large bird impacts.

TABLE 4

TENTATIVE COMPUTER RUN MATRIX

Equivalent Experimental Data (Shot No.)	Impact Angle (Degrees)	Nominal Bird Size (grams)	Impulse Level	Loading* Conditions
40138	90	77	Low	1T, 2T, 1S, 2S
40049	90	77	Intermediate	1T, 2T, 1S, 2S
40078	90	77	High	1T, 2T, 1S, 2S
40048	90	560	High	1T, 2T, 1S, 2S
40092	45	77	Low	OBM**
40083	45	77	High	OBM
40085	45	560	High	OBM
40117	25	77	Low	OBM
40139	25	77	Intermediate	OBM
40116	25	77	High	OBM
40120	25	560	High	OBM

*Reference Paragraphs 3.1.1 and 4.3.1.

**Oblique Incidence Model.

TABLE 5

COMPUTER RUN MATRIX FOR WHICH RESULTS ARE PRESENTED

Equivalent Experimental Data (Shot No.)	Impact Angle (Degrees)	Nominal Bird Size (grams)	Impulse Level	Loading* Conditions
40138	90	77	Low	1T, 2T, 1S, 2S
40049	90	77	Intermediate	1T, 2T, 1S, 2S
40092	45	77	Low	OBM**
40083	45	77	High	OBM
40117	25	77	Low	OBM
40139	25	77	Intermediate	OBM

*Reference Paragraphs 3.1.1 and 4.3.1.

**Oblique Incidence Model.

SECTION 4
LOAD MODEL EVALUATION

Evaluation of the loading models as a function of the panel response level was achieved by comparing the analytical results with the corresponding experimental results. To facilitate this a number of adjustments in the data had to be made. The most significant of these are discussed in paragraphs 4.1 and 4.2. The discussion associated with the load model evaluation is then presented in paragraph 4.3.

4.1 SYNCHRONIZATION OF IMPACT TIME

The out-of-plane displacement data was recorded with a high speed framing camera giving a time resolution of 150 microseconds. For the nominal 77 gram bird (length = 7.62 cm; diameter = 3.81 cm) the duration of the loading phase of the impact event at the higher velocities is approximately 300 microseconds. Thus, in order to compare response data it is necessary to synchronize the time after impact for the experimental data with the analytical data.

The incremental time adjustment in the experimental data was calculated using a two step graphical extrapolation procedure. For a given set of experimental data the time history of panel displacement, w, along the panel center-line was plotted as depicted in Figure 17. Representative points were then selected (denoted as x_1, x_2, and x_3 on Figure 17) for cross-plotting as shown in Figure 18. These points were then fitted with a curve and extrapolated to zero displacement. A best estimate of ΔT was then defined and was used to locate the time of impact between frame zero (the last frame showing no displacement) and frame one on the film data.

4.2 IMPACT LOCATION

Because of deviations in the line of flight of the projectile the designated impact point and the actual impact

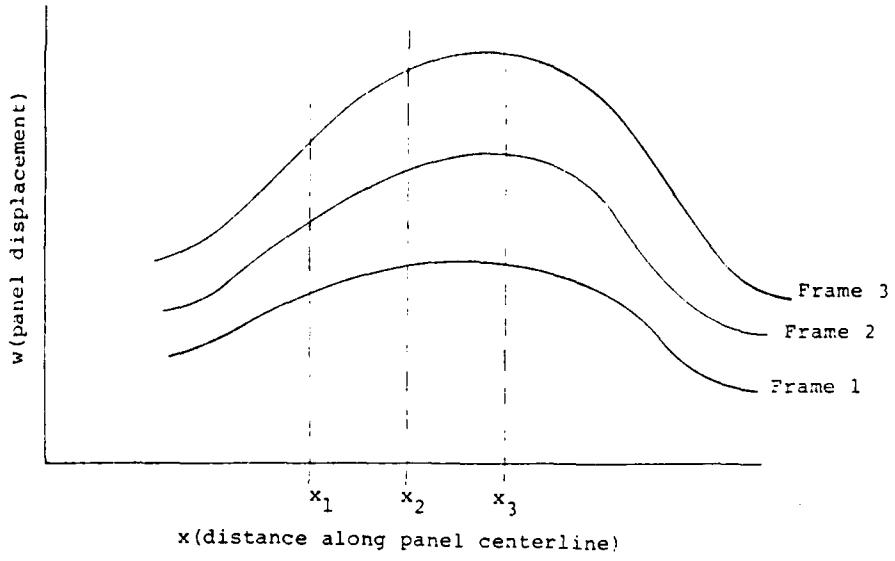

Figure 17. Displacement Time History Along Panel Centerline.

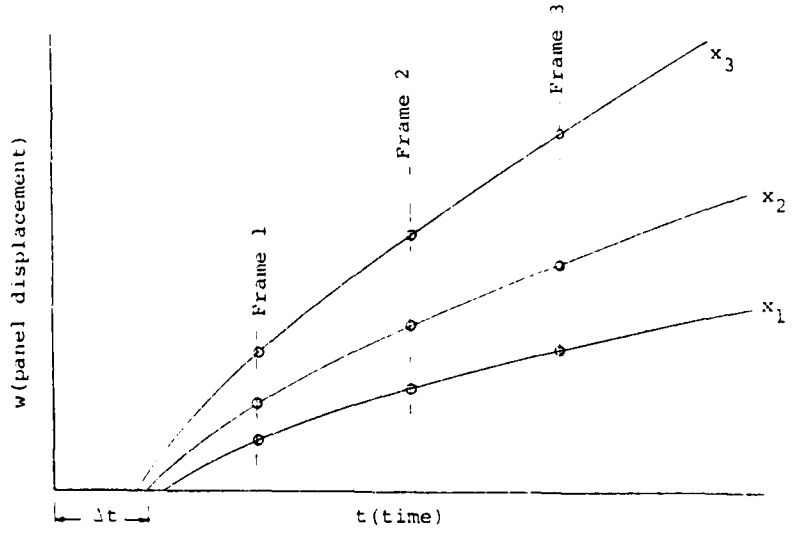

Figure 18. Displacement Time History of Selected Panel Locations.

point are not always coincident. For most cases the maximum deviation measured in a plane normal to the centerline of the gun was less than one centimeter. However, for the 25 degree oblique impacts this translates into a maximum deviation measured along the surface of the panel of about 2.4 cm (1 inch).

For the normal impact conditions the response was symmetrical. In these cases the experimental data was simply aligned with the computed data using the known condition of symmetry.

For the oblique impact cases it was necessary to compute a shift factor for the experimental data to make the actual center of impact correspond to the center of impact for the computed data (all impacts were at the theoretical impact point for the computed data). This shift factor was determined using scaled measurements taken from the moire' fringe film data and measurements taken from the actual hardware of the individual test panels.

4.3 COMPARISON OF EXPERIMENTAL AND ANALYTICAL RESULTS

Evaluation of the load model to meet the program objective was accomplished through a comparison of the analytical and experimental results. This effort is documented as a function of impact angle and impacting energy in the subsequent paragraphs.

4.3.1 Normal Impact ($\theta = 90°$)

a) Experimental Shot No. 40138

Analytical response calculations were made for four different loading conditions for comparison with the experimental data. The loading conditions were: (1) square wave temporal loading with a uniform spatial distribution over one bird diameter (1-S); (2) square wave temporal loading with a uniform spatial distribution over two bird diameters (2-S); (3) triangular temporal loading with a uniform spatial

distribution over one bird diameter (1-T), and; (4) a triangular temporal loading with a uniform spatial distribution over two bird diameters (2-T). The small bird size (86.2g) and low impact velocity (72 m/sec) associated with this test point represent a relatively low energy level impact.

The results are presented for three successive times after impact on Figures 19, 20, and 21. The x-coordinate is measured along the centerline of the panel in the lengthwise direction with 0.0 being the center of the panel. Examination of these figures indicates that the one bird diameter spatial load models result in excessive localized response with the triangular pulse being more severe than the square pulse. The response shape for the two bird diameter spatial load models is generally good. However, the magnitude of the response for the square pulse shows better agreement with the experimental data than does the triangular pulse.

The peak response level at all computed times for all load models is higher than the measured experimental results. This is illustrated graphically on Figures 22 and 23 for the two diameter spatial load models at x = 76 mm and x = 0.0 mm. The time in these plots is normalized with respect to the loading time of the bird, L/V.

The incremental difference between the square pulse load model and the experimental data at x = 76 and is relatively constant with respect to time and the percentage difference decreases from about 35% to 15% with increasing time. The time shift required to make the computed values for the square pulse model and the experimental data coincide is about 1.05 frames. Thus, error in synchronization of the impact times (Ref. paragraph 4.1) could account for some of this difference (the estimated synchronization time is felt to be accurate to within 20 percent for this case).

The difference between the square pulse load model and the experimental data at x = 0 is about constant at

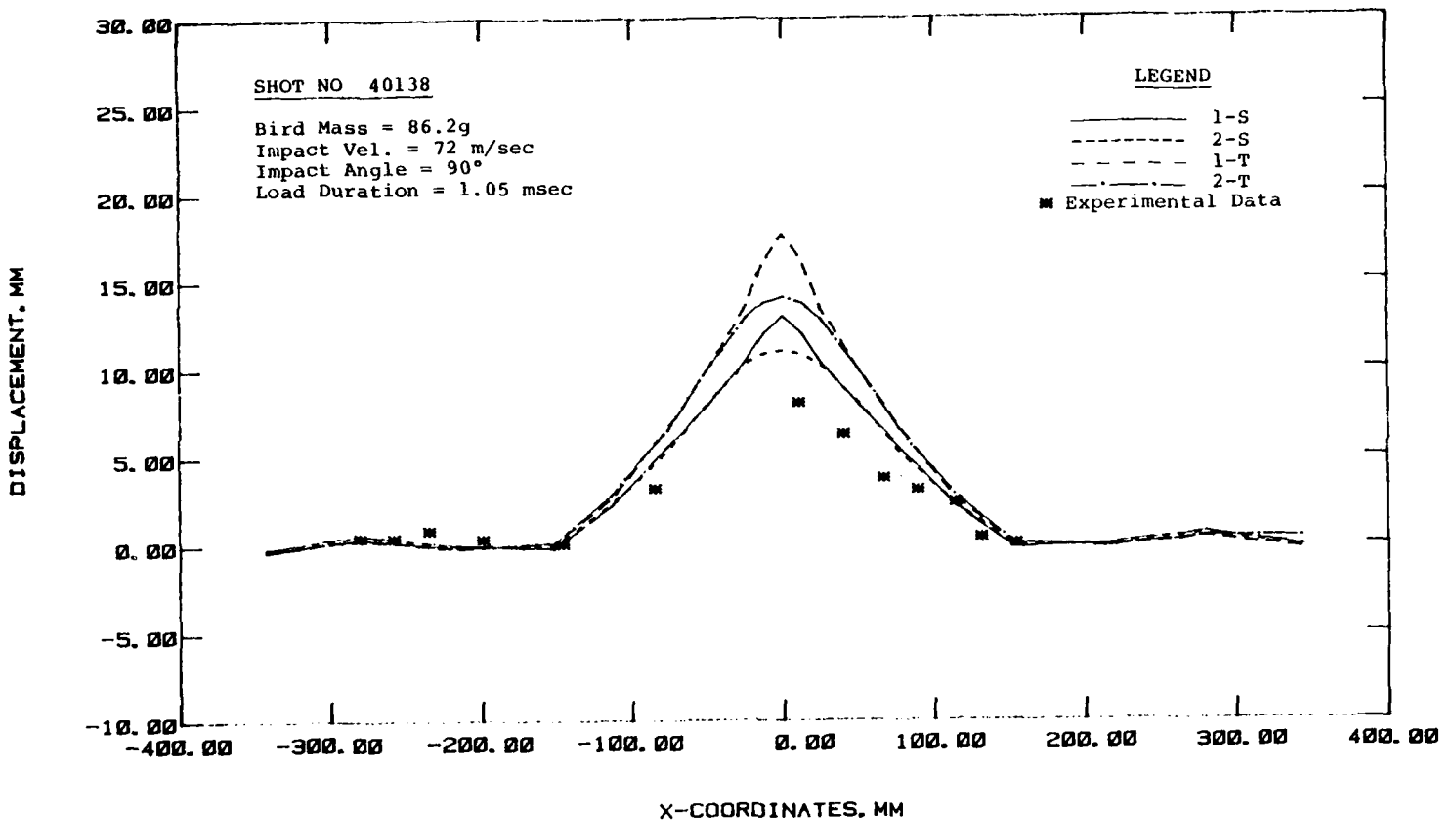

Figure 19. Comparison of Analytical and Experimental Results for Shot No. 40138 at t = .535 msec.

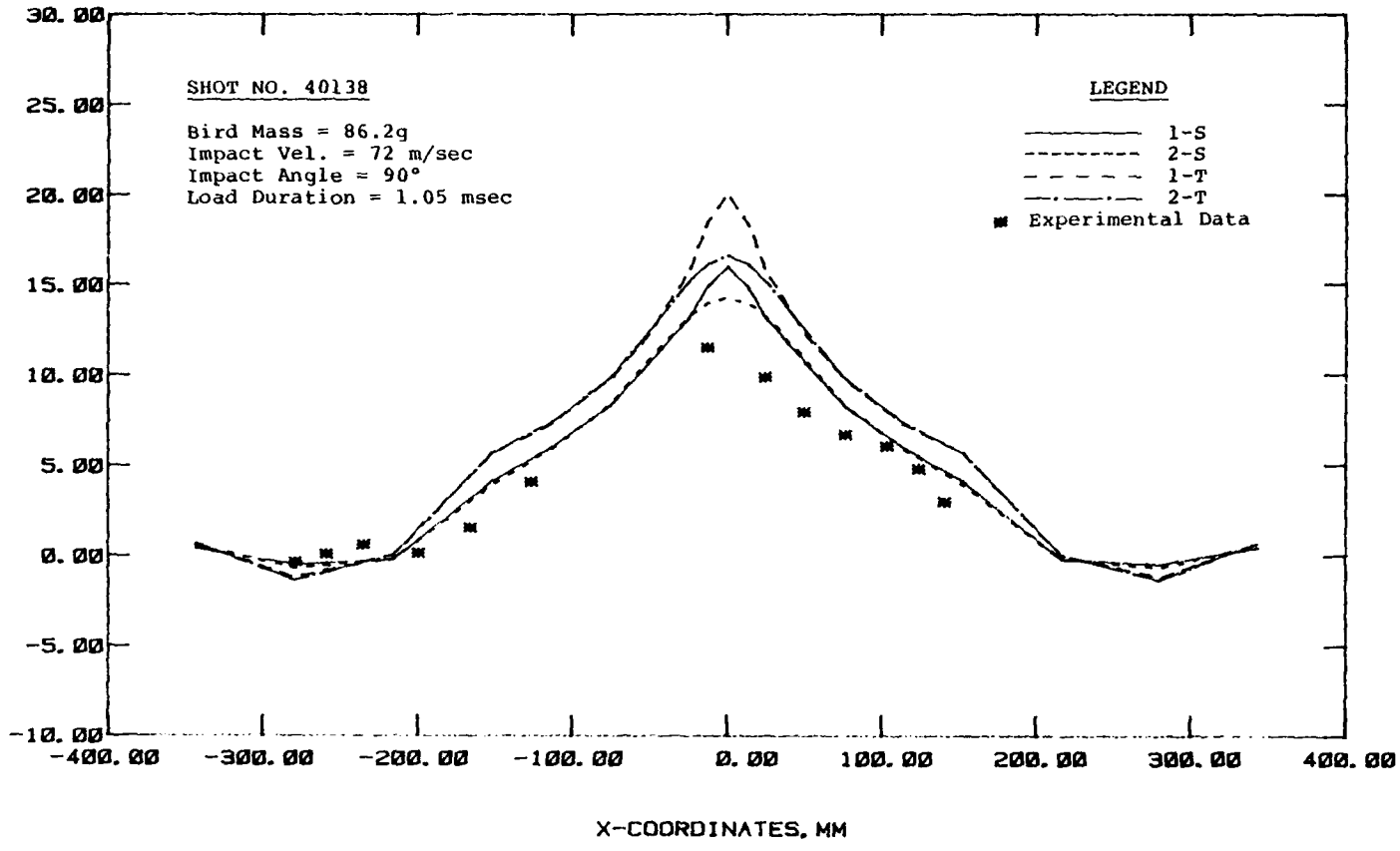

Figure 20. Comparison of Analytical and Experimental Results for Shot No. 40138 at t = .827 msec.

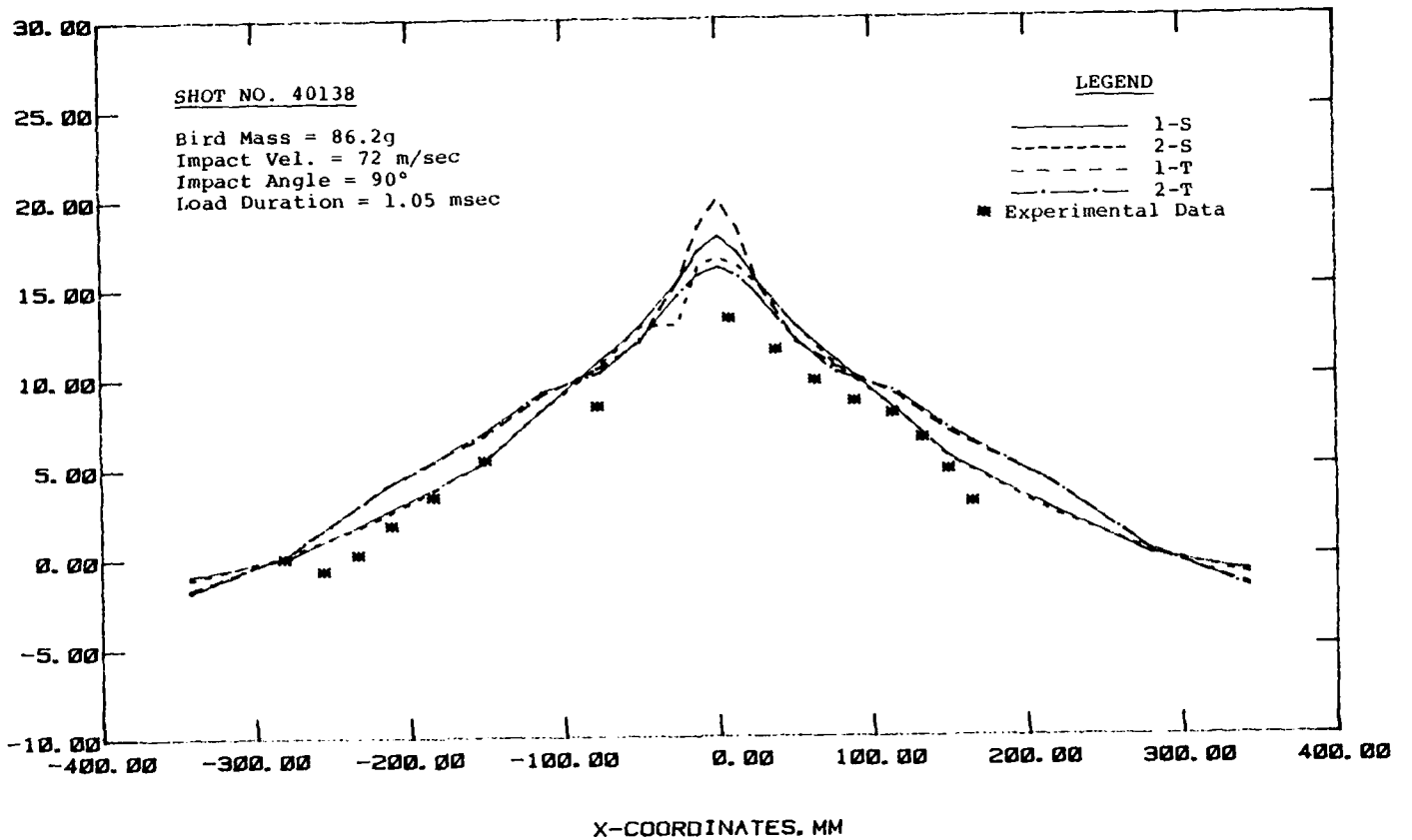

Figure 21. Comparison of Analytical and Experimental Results for Shot No. 40138 at t = 1.119 msec.

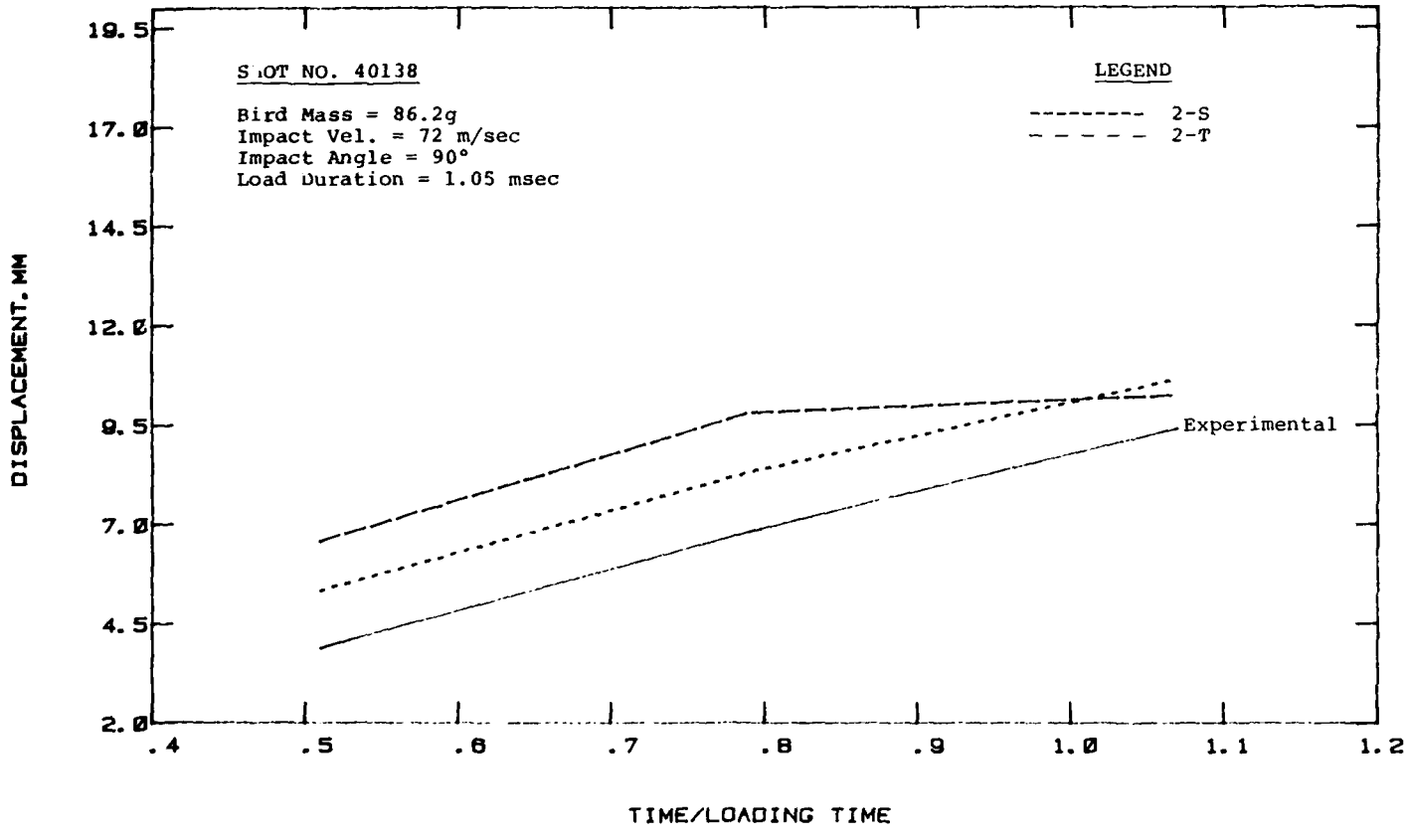

Figure 22. Comparison of Panel Displacement vs. Time for Shot No. 40138 at Sta. x = 76 mm.

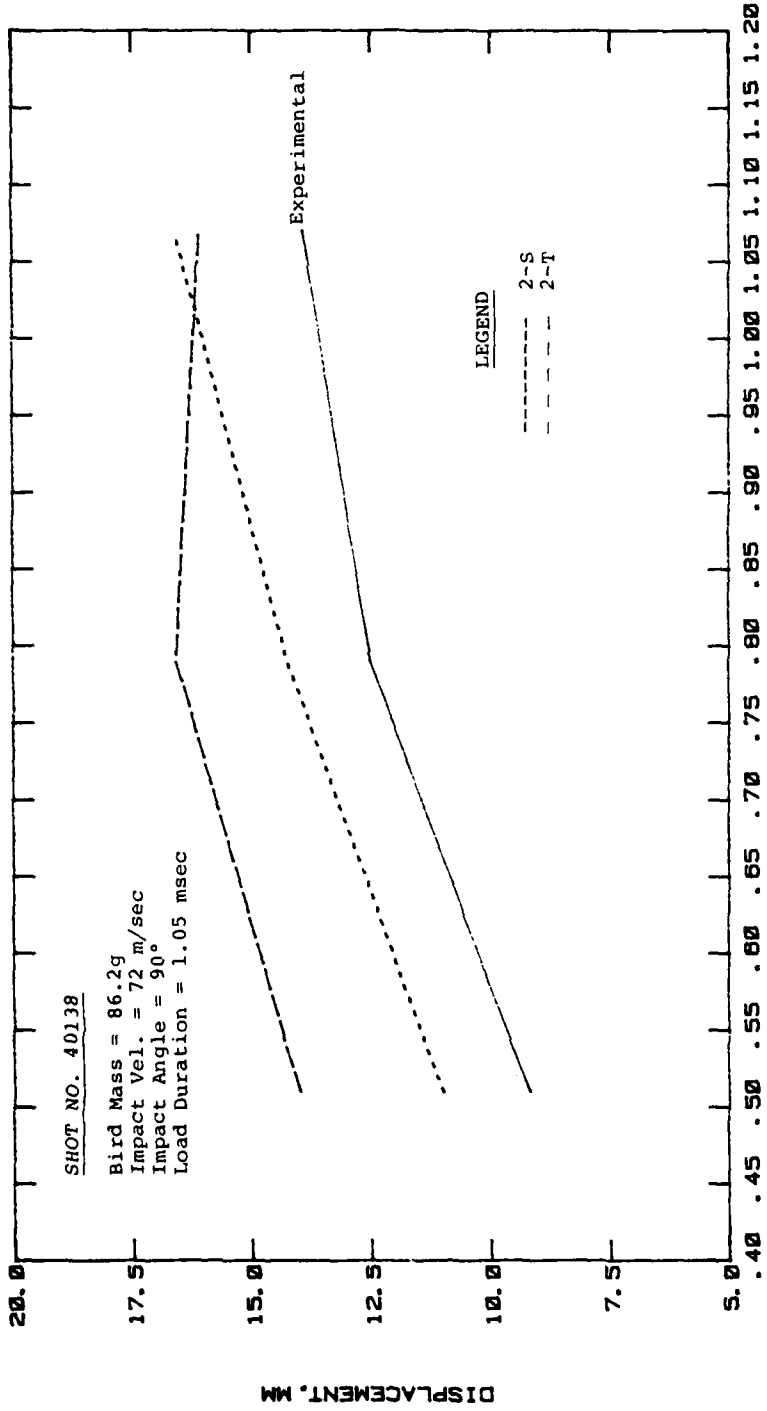

Figure 23. Comparison of Panel Displacement vs. Time for Shot No. 40138 at Sta. x = 0.0 mm.

15-20 percent. The experimental data for this plot was obtained by estimating the deflected shape at the peak displacement because, in general, fringes did not occur at x = 0.

The differences associated with the triangular pulse model is greater at early times indicating that the load is increasing too rapidly. However, the calculated results are convergent with respect to the experimental results as the time approaches the loading time.

In summary, the two bird diameter loaded area models show reasonable agreement with the square pulse being somewhat better over the time range investigated. Additional refinements in the load model (such as increasing the loaded area) could be expected to provide close correlation between computed and experimental data for the impact conditions represented by this shot.

b) Experimental Shot No. 40049

As a result of the comparisons made for Shot No. 40138, analytical calculations for this shot were limited to the 2-S and 2-T loading models. The bird size (84.7g) and impact velocity (155 m/sec) associated with this shot represent an intermediate energy level impact.

Displacement along the panel centerline for successive times are shown on Figures 24 through 27. The time history of displacement at three panel locations is shown in Figures 28 , 29 , and 30 .

Examination of the experimental data presented on these plots reveals a very rapid build-up of local deformation under the point of impact. The peak magnitude of this local pocketing then remains relatively constant at 25-30 mm throughout the duration of the loading event (Reference Figure 28). Additional energy is absorbed through an increase in diameter of the deformed area. This increase progresses at a somewhat constant rate (Reference Figures 29 and 30) until

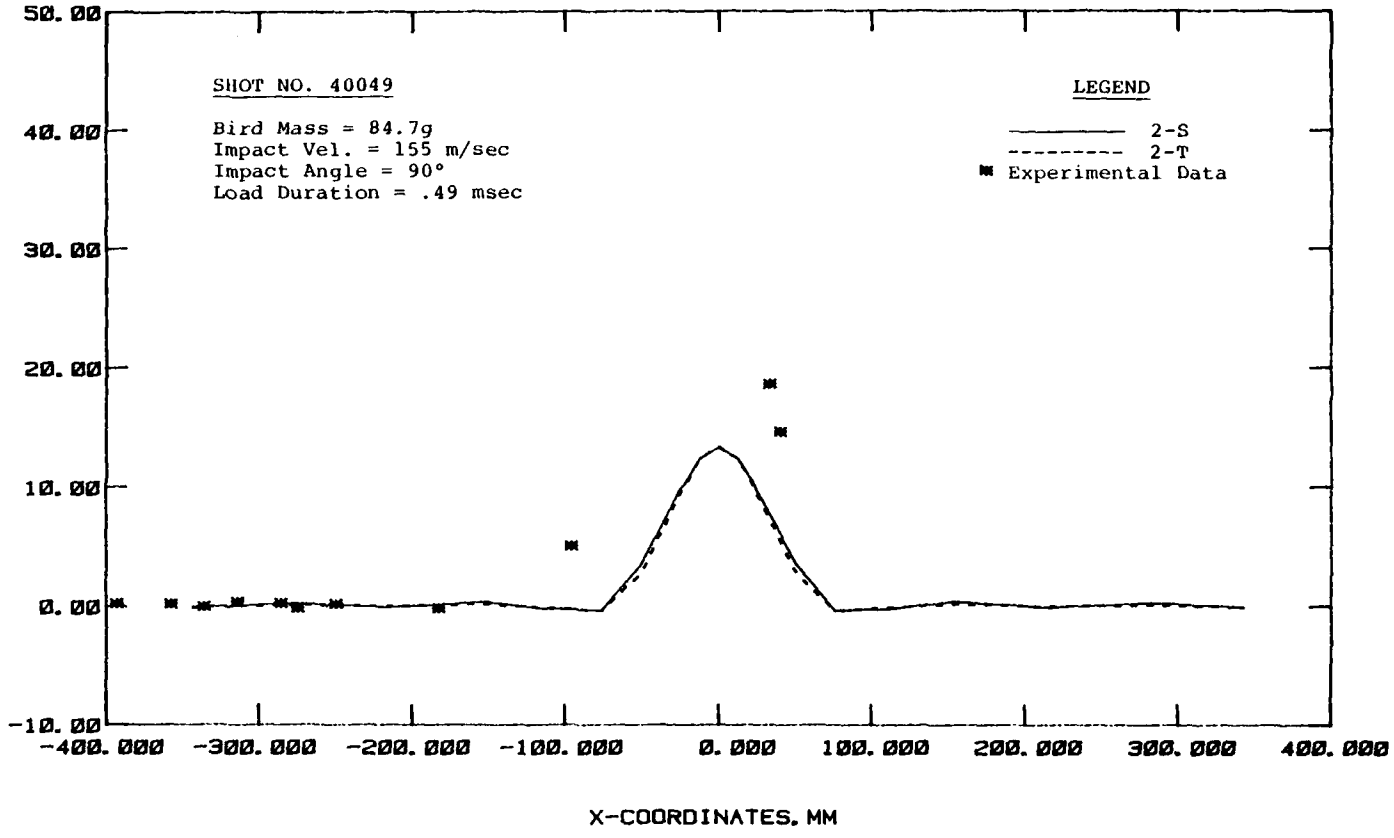

Figure 24. Comparison of Analytical and Experimental Results for Shot No. 40049 at t = .1384 msec.

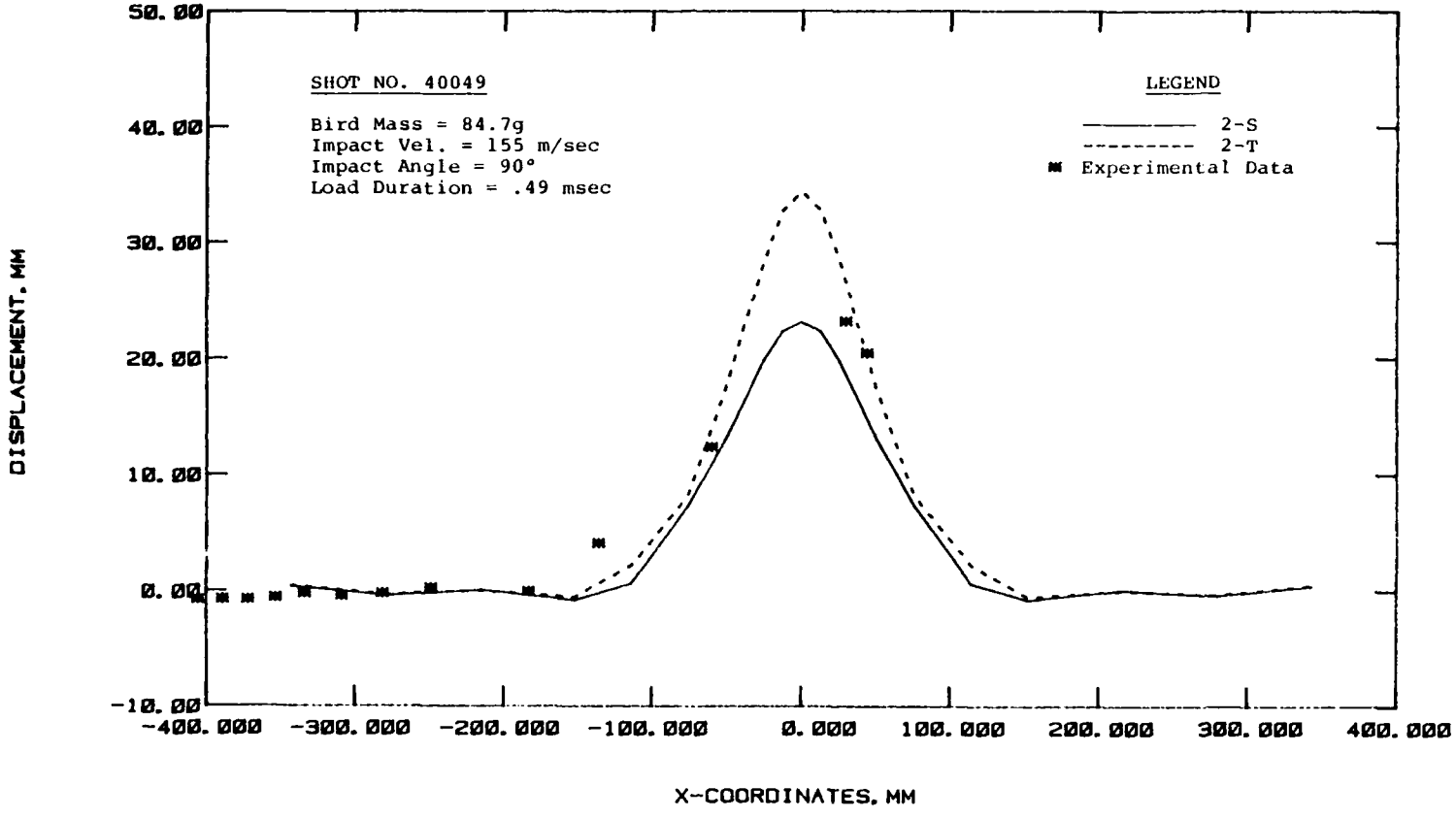

Figure 25. Comparison of Analytical and Experimental Results for Shot No. 40049 at t = .2918 msec.

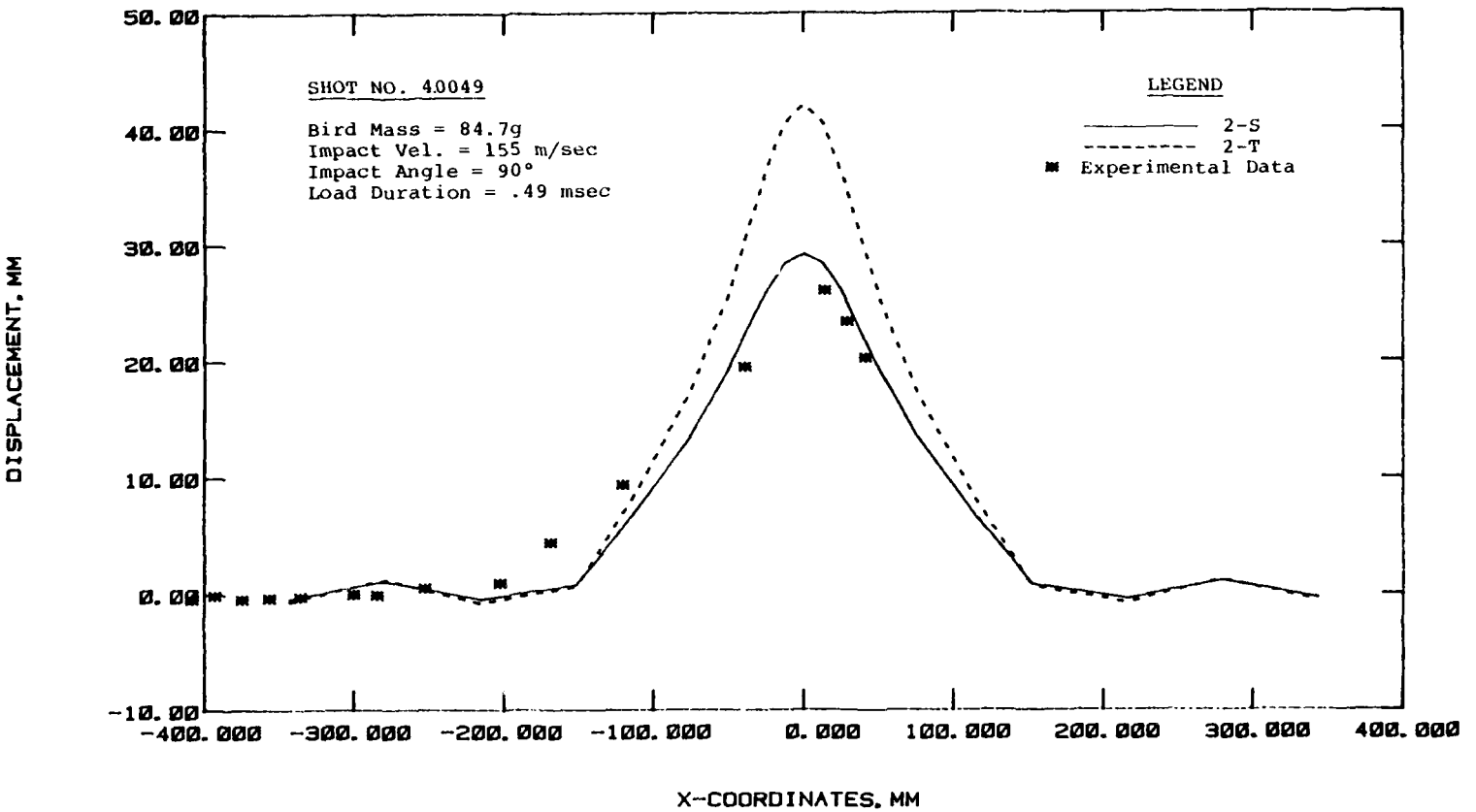

Figure 26. Comparison of Analytical and Experimental Results for Shot No. 40049 at t = .4452 msec.

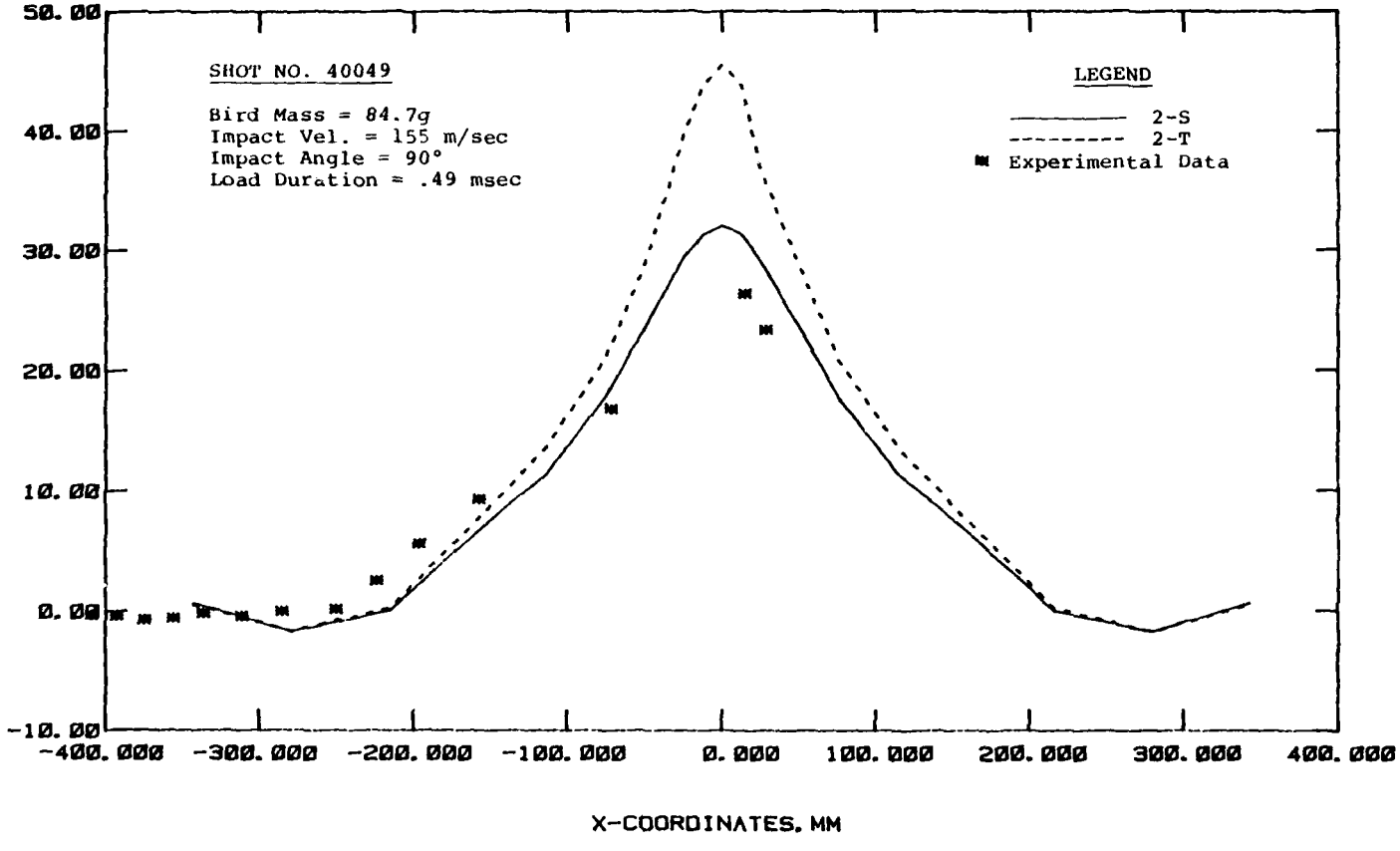

Figure 27. Comparison of Analytical and Experimental Results for Shot No. 40049 at t = .5986 msec.

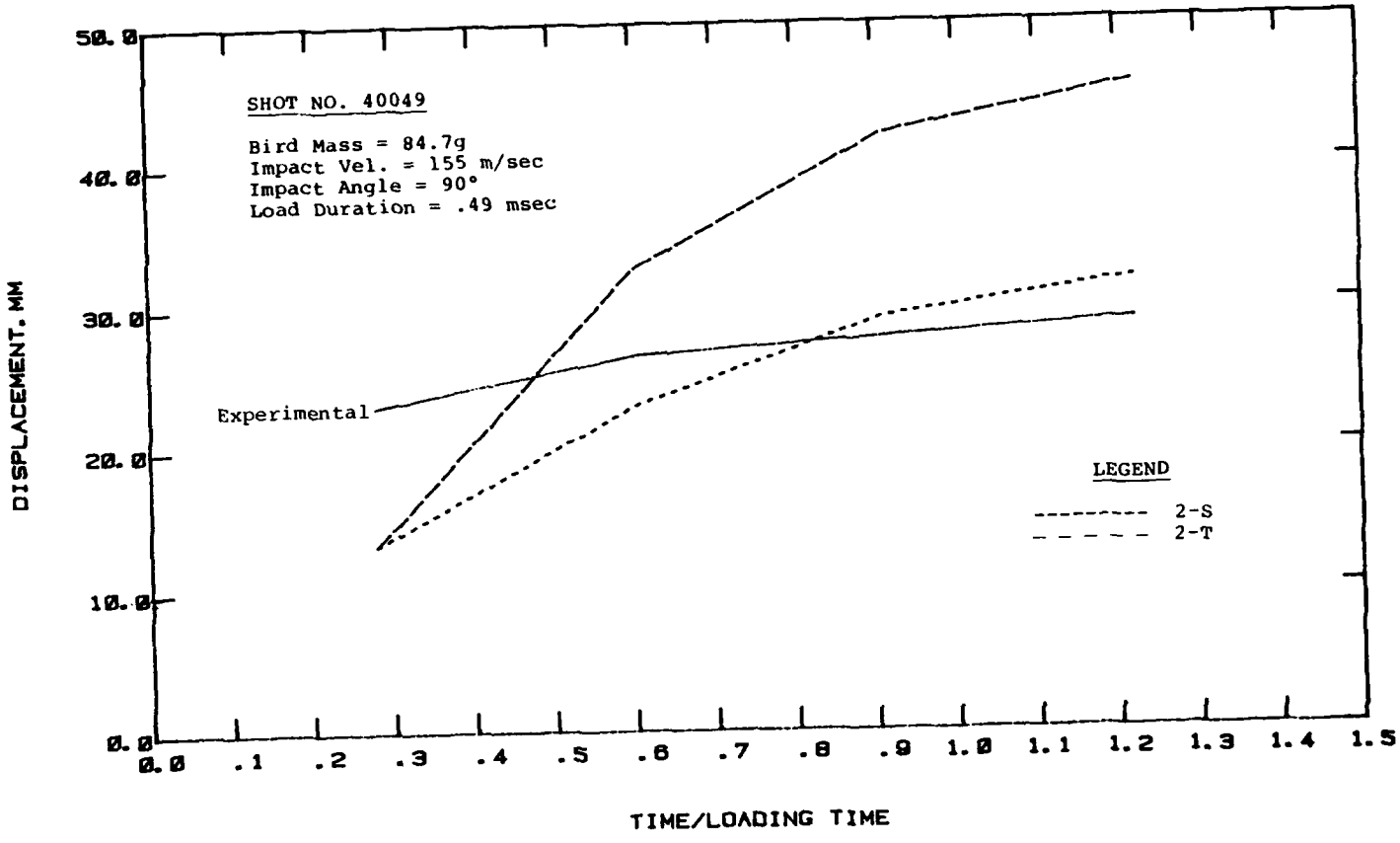

Figure 28. Comparison of Panel Displacement vs. Time for Shot No. 40049 at Sta. x = 0.0.

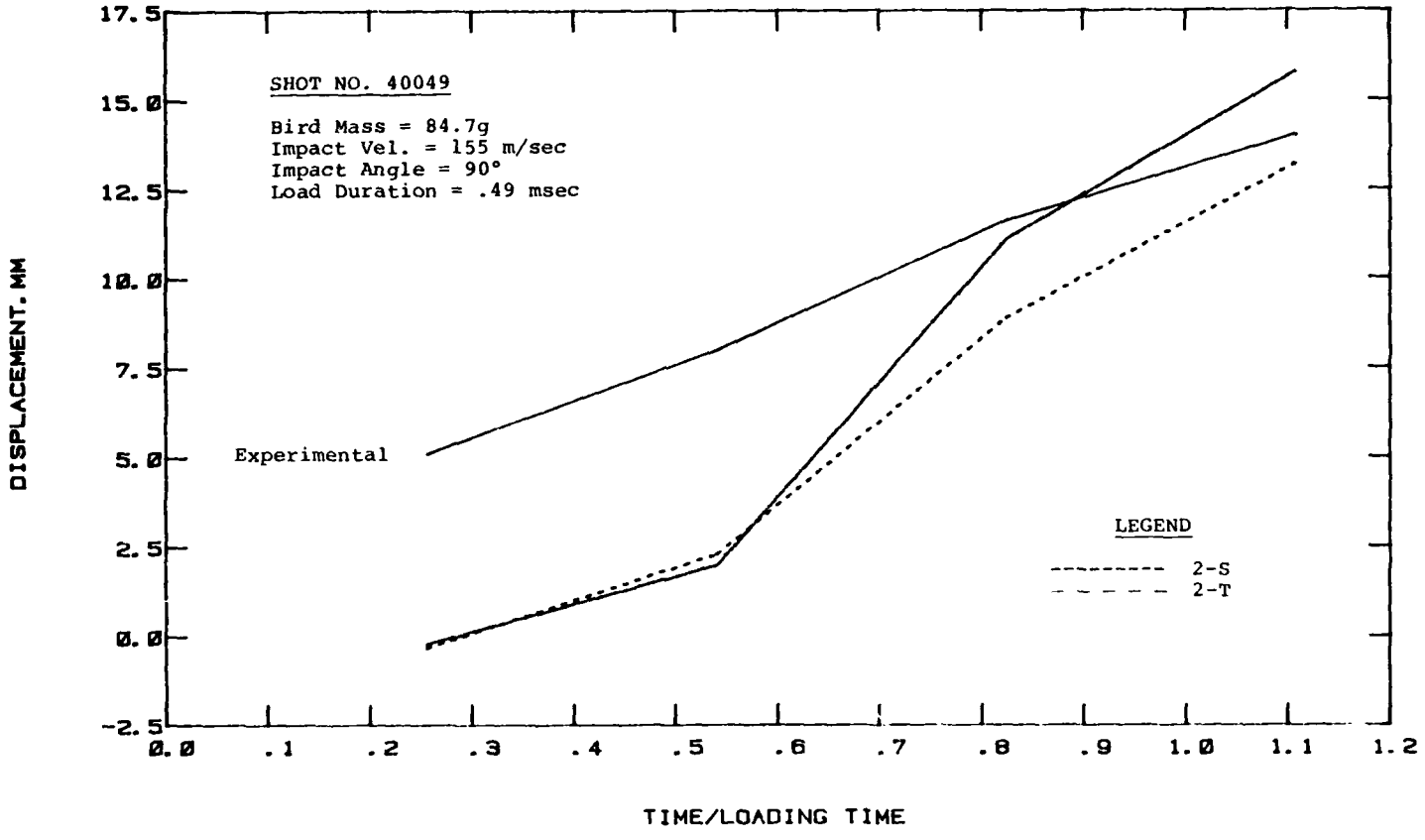

Figure 29. Comparison of Panel Displacement vs. Time for Shot No. 40049 at Sta. x = -95 mm.

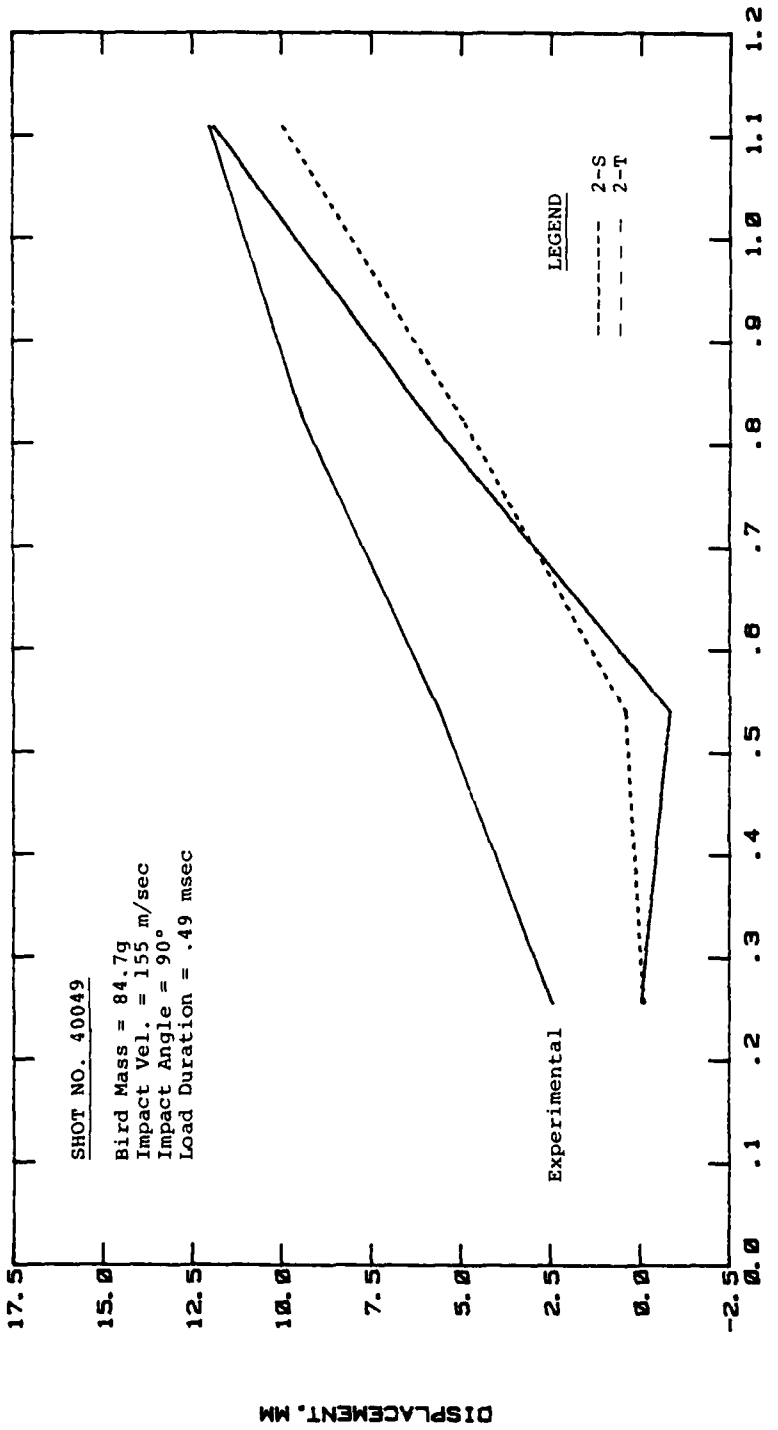

Figure 30. Comparison of Panel Displacement vs. Time for Shot No. 40049 at Sta. x = -120 mm.

a pocket diameter of approximately 400 mm (16 inches) is attained at a time of 0.6 msec (t/T = 1.22) as shown on Figure 27.

Neither the 2-T or 2-S load model predicts the rapid build-up of local deformation at the center of impact. The 2-T load model ultimately over predicts the magnitude of the local deformation at the point of impact by a large margin as shown on Figure 28. The magnitude of local deformation predicted by the 2-S model is in good agreement with the experimental results for times corresponding to t/T greater than 0.5. Both loading models underestimate the rate of growth of the local bulge diameter as shown by Figure 29 and 30.

In summary, the 2-S load model predicts the panel response better than the 2-T model. Although the 2-S model predicts behavior reasonably well, it is apparent that there are significant differences. Furthermore, it appears that the refinements to the model to achieve close agreement between experimental and analytical results would be more complex than for the lower energy impact condition.

4.3.2 Oblique Impact ($\theta \approx 45°$)

a) Experimental Shot No. 40092

Analytical data was generated for the 45° oblique angle impacts using the uncoupled loading model described in paragraph 3.1 of this report and in Reference 2. The impact mass (76.7g), velocity (99 m/sec) and 45 degree impact angle associated with this shot represent a low level impact condition. The maximum deflection (measured from the experimental data) continued to increase to a maximum of about 11 mm at t/T = 0.93. There was no significant permanent deformation in the panel after the impact.

---

[2] J. P. Barber, H. R. Taylor and J. S. Wilbeck, Bird Impact Forces and Pressures on Rigid and Compliant Targets. (AFFDL-TR-77-60, ADA061-313, May 1978.)

The perimental and analytical results for the centerline displacement at successively increasing times are shown in Figures 31 through 35. The loading model predicts a more localized response than was measured experimentally. The location of the peak displacement is at about x = 13 mm for the analytical results and does not vary with time (the bird impacts from the positive x-direction). For the experimental data the location of the peak displacement varies from x = 36 mm at t/T = 0.11 to x = -20 mm at t/T = 0.66. Examination of the experimental data (not presented here) reveals that the point of peak displacement continues to move and is located at x = -125 mm when t/T is 1.5.

The peak displacement as a function of time is shown in Figure 36 (these plotted values do not occur at the same point on the panel). Examination of this figure together with Figures 31 through 35 indicates that the agreement of the experimental and analytical results with respect to both shape and magnitude improves with increasing time.

In summary, it appears that for the impact conditions represented the loading model exhibits deficiencies with respect to deflected shape, response magnitude, and location of the peak displacement.

b) Experimental Shot No. 40083

A comparison of the analytical and experimental results for successive times is presented in Figures 37, 38, and 39. The bird mass of 80.1g together with the impact velocity of 257 m/sec represents a high energy impact condition. This is evidenced by the large deflections shown on these Figures and by the 1.25 inch deep plastic pocket in the tested panel.

The shape of the response shows good agreement. However, the problem of analytically predicting the location of the peak displacement is again evident.

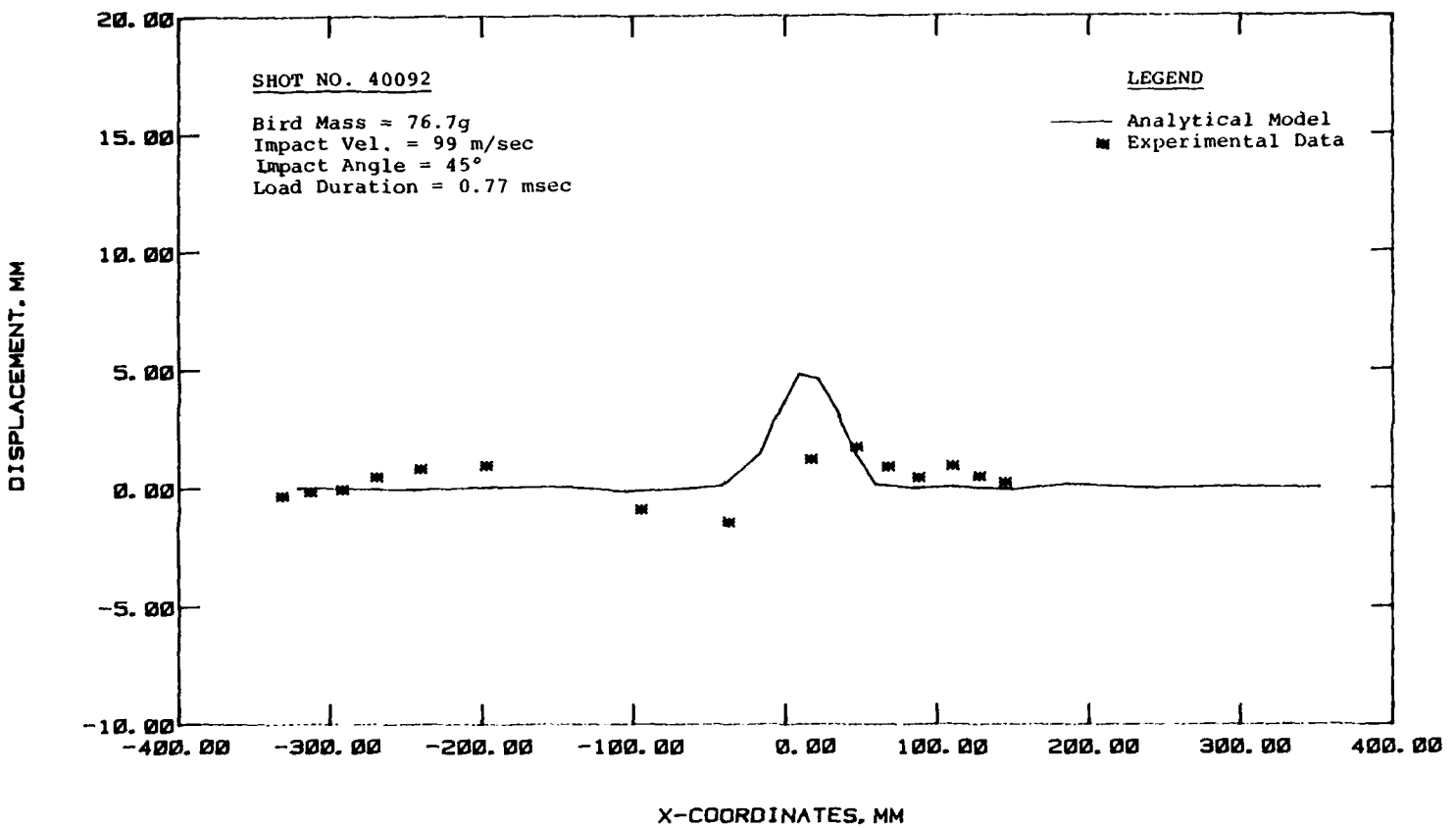

Figure 31. Comparison of Analytical and Experimental Results for Shot No. 40092 at t = .131 msec.

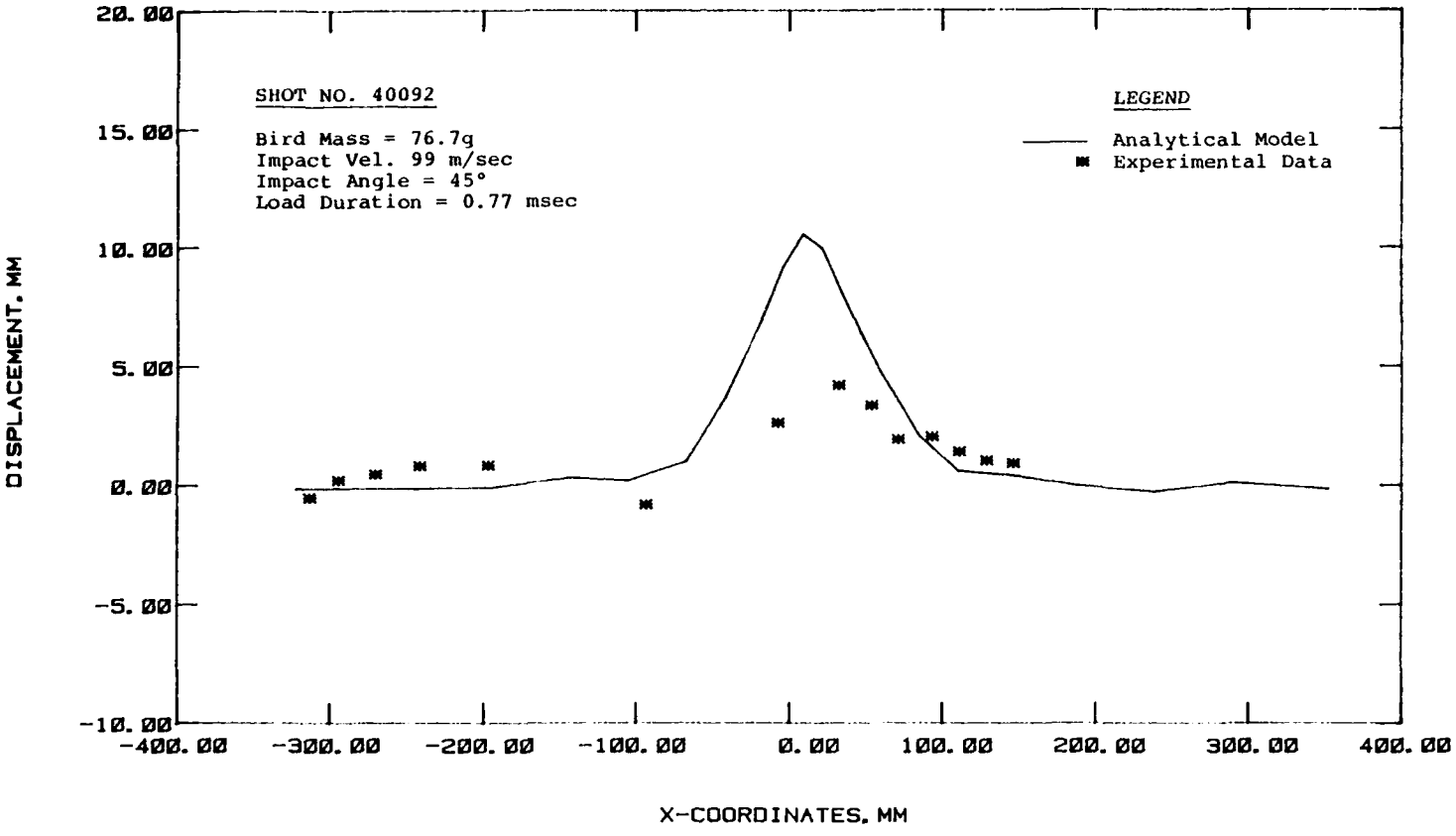

Figure 32. Comparison of Analytical and Experimental Results for Shot No. 40092 at t = .290 msec.

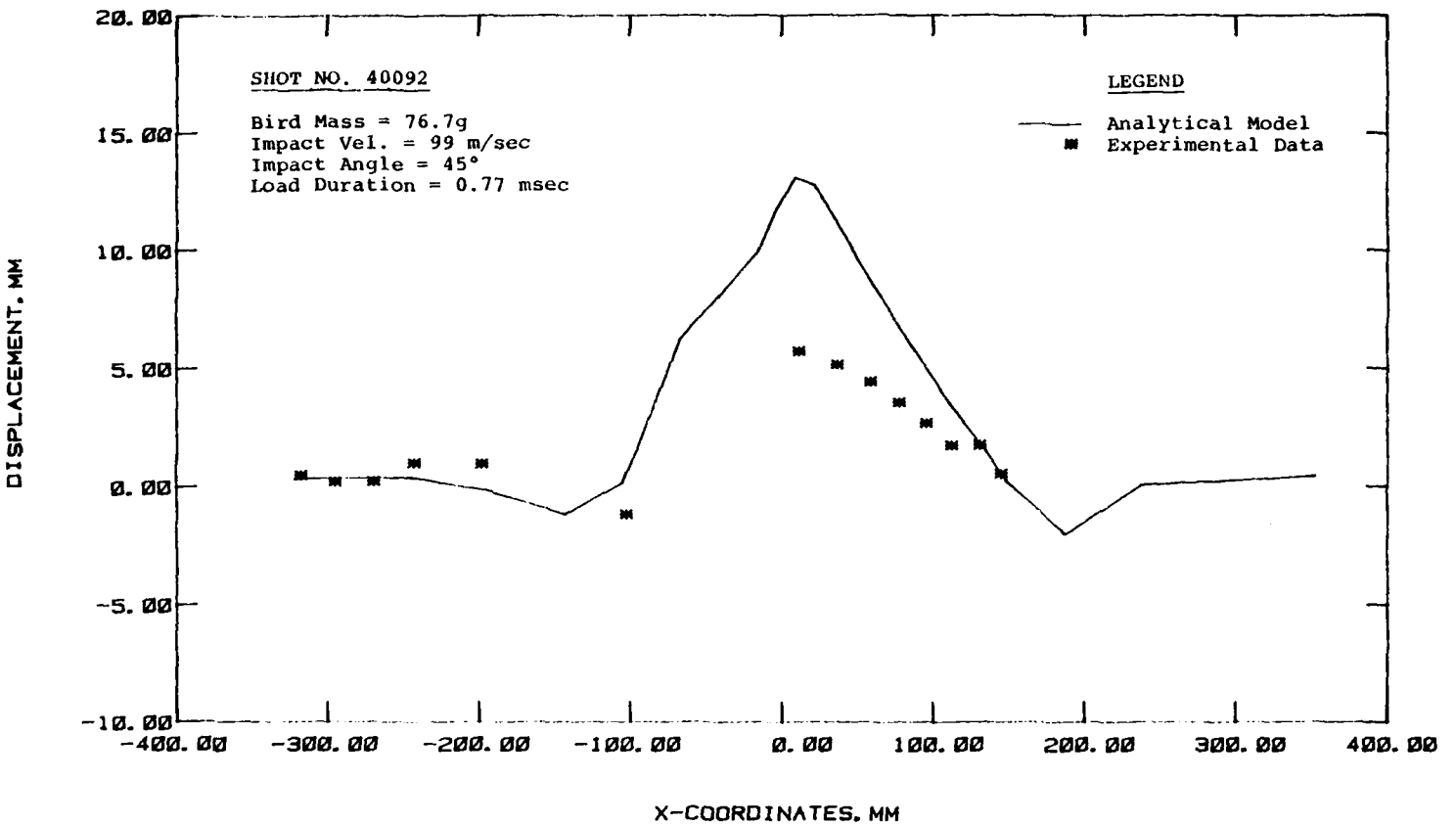

Figure 33. Comparison of Analytical and Experimental Results for Shot No. 40092 at t = .449 msec.

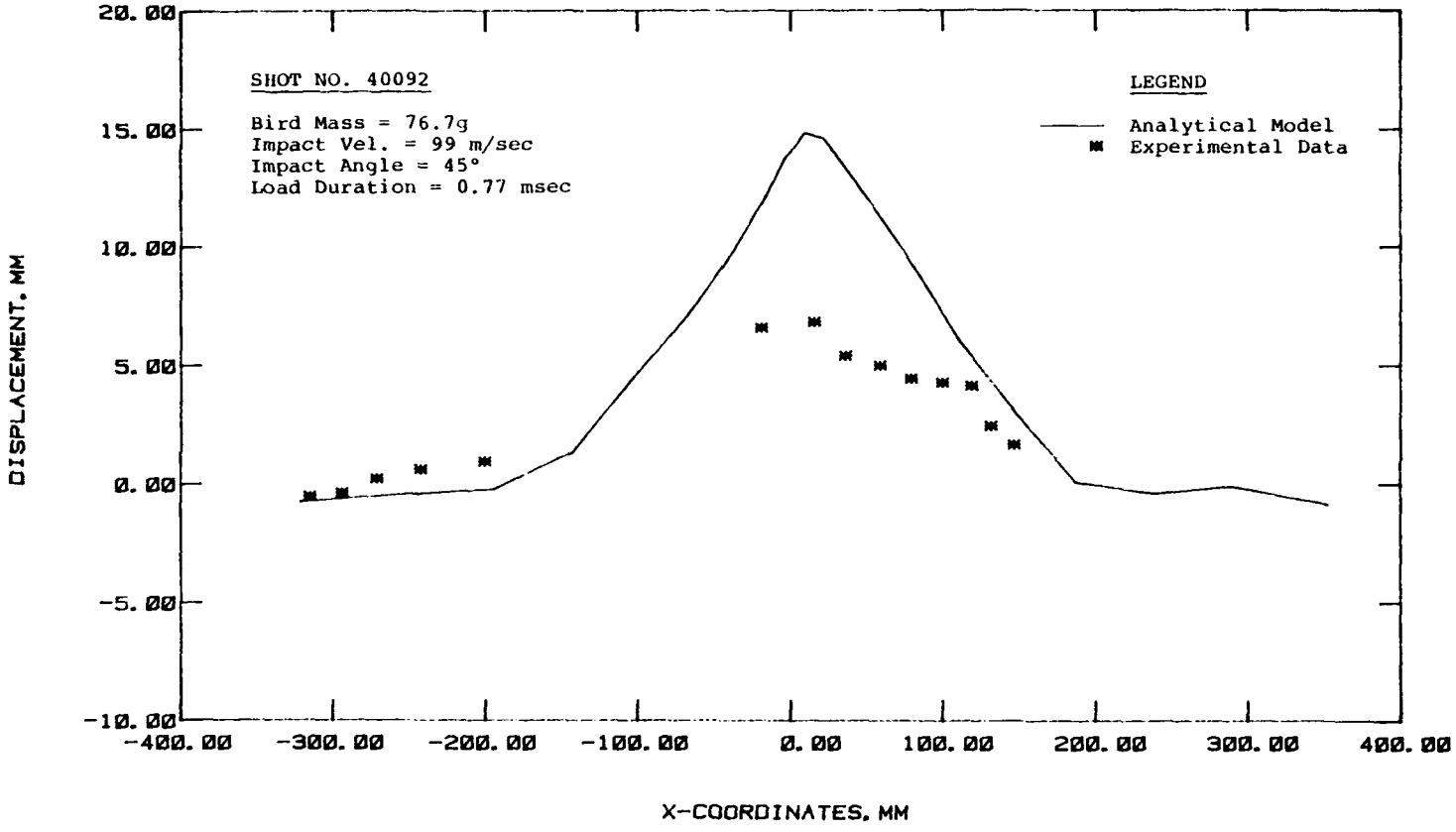

Figure 34. Comparison of Analytical and Experimental Results for Shot No. 40092 at t = .607 msec.

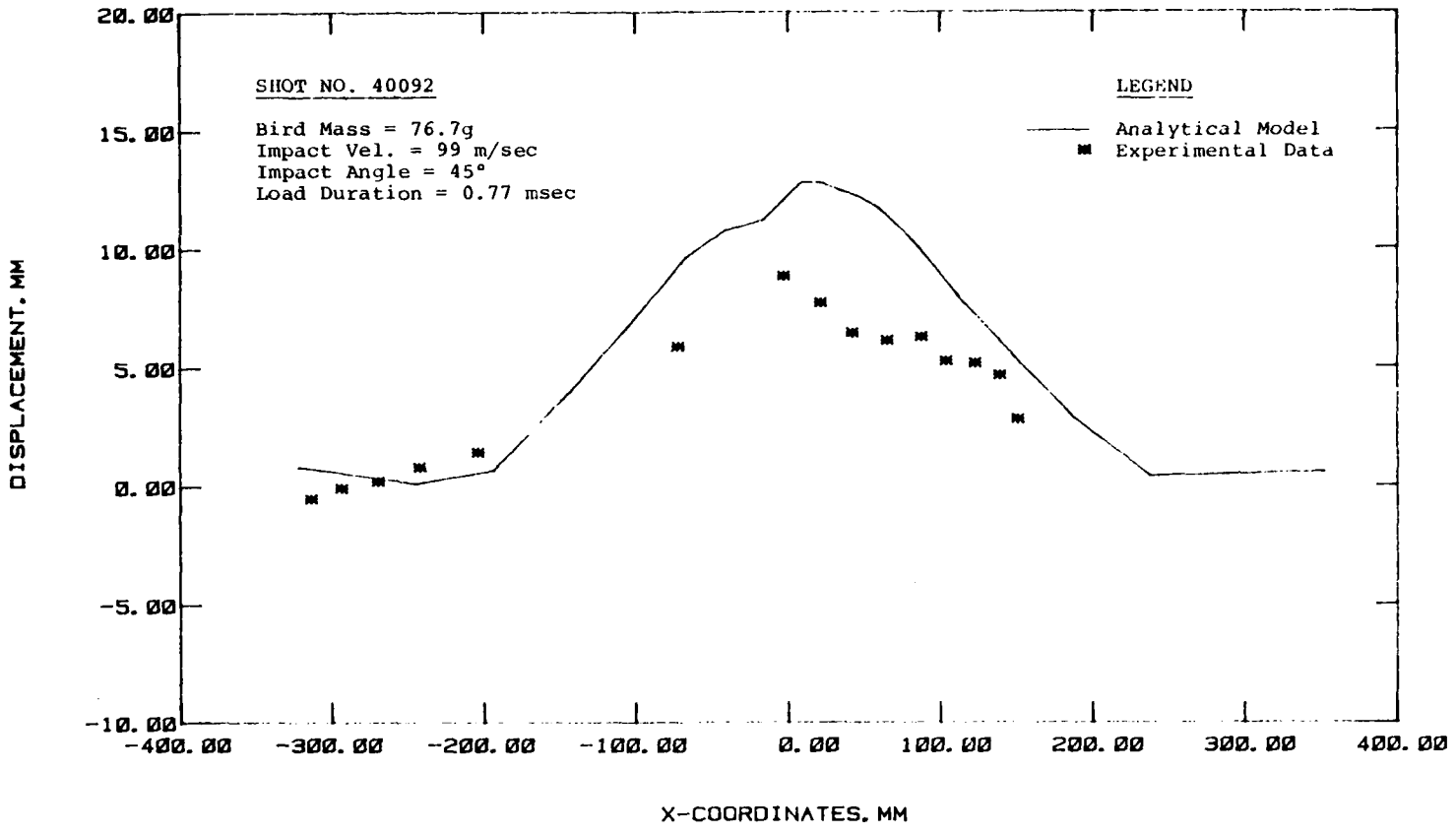

Figure 35. Comparison of Analytical and Experimental Results for Shot No. 40092 at t = .763 msec.

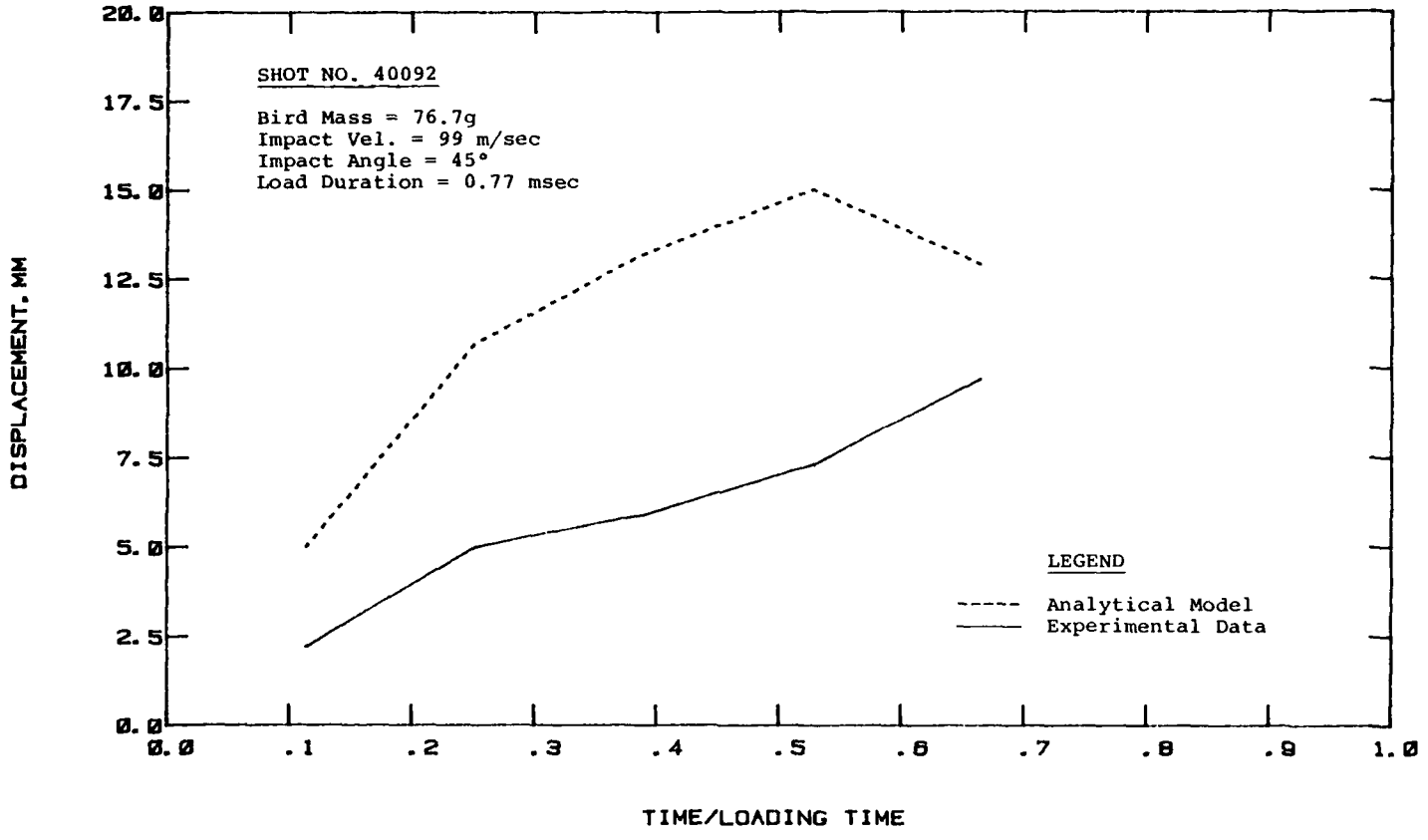

Figure 36. Comparison of Peak Panel Displacement vs. Time for Shot No. 40092.

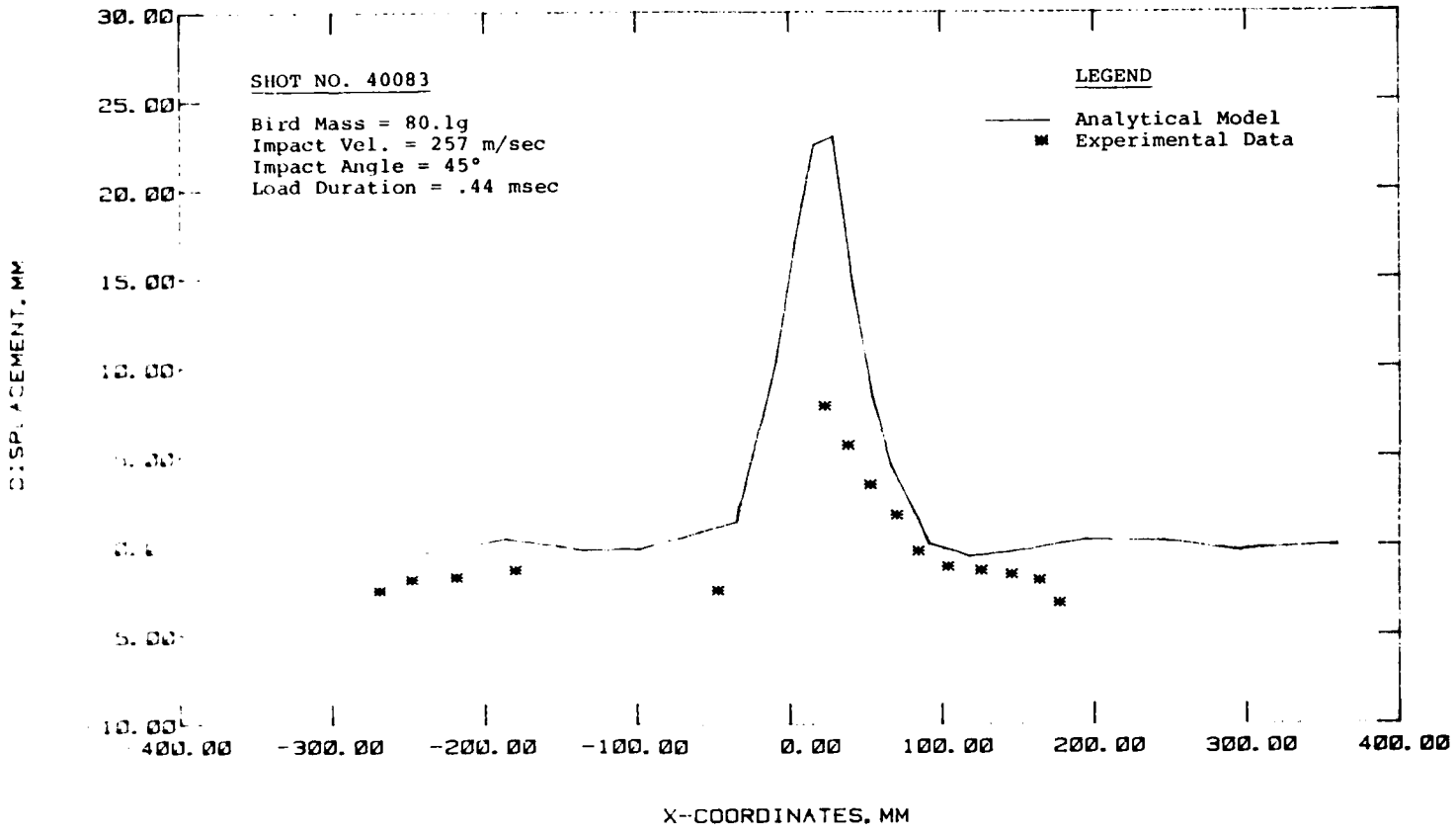

Figure 37. Comparison of Analytical and Experimental Results for Shot No. 40083 at t = 0.108 msec.

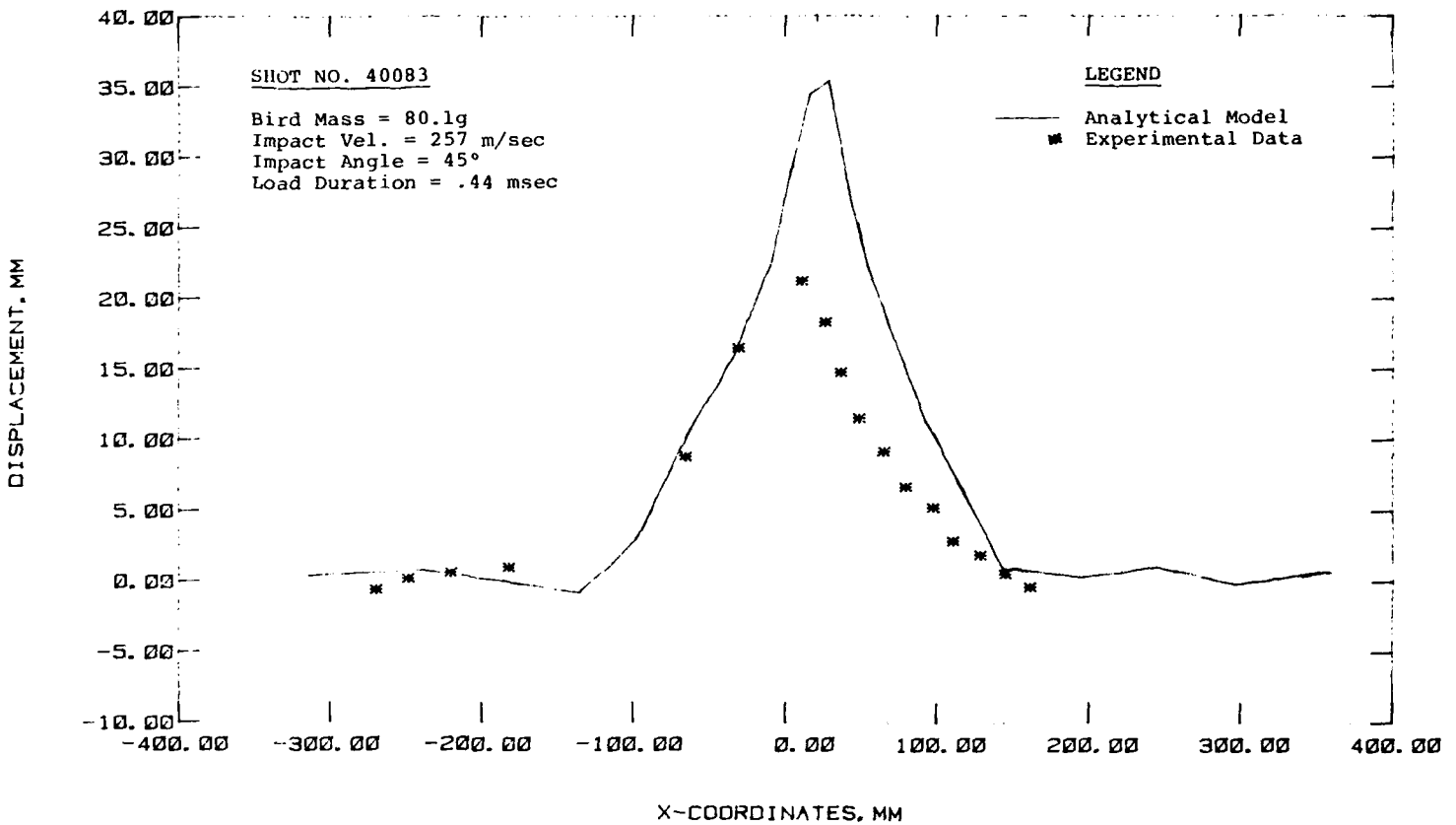

Figure 38. Comparison of Analytical and Experimental Results for Shot No. 40083 at t = 0.265 msec.

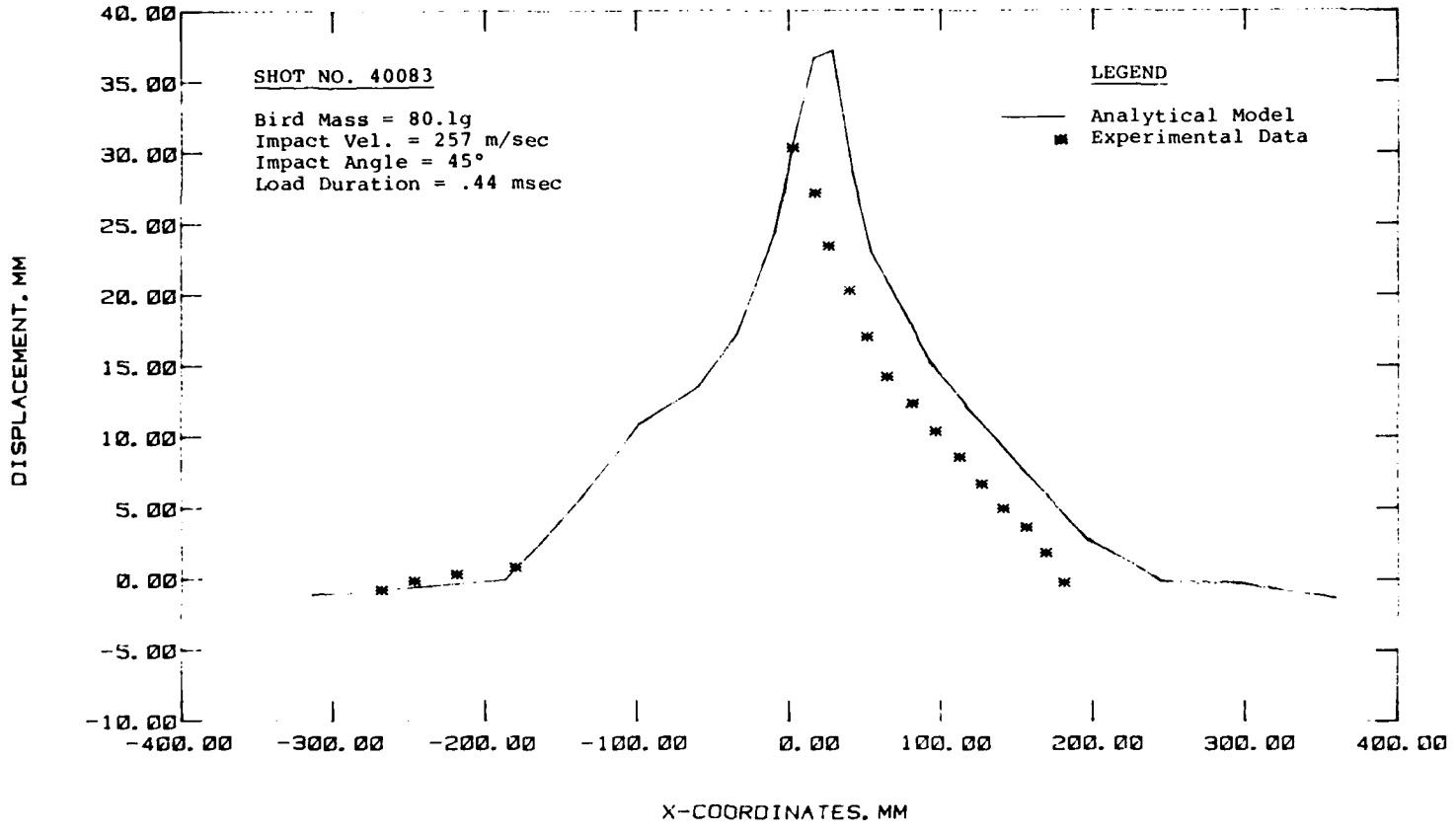

Figure 39. Comparison of Analytical and Experimental Results for Shot No. 40083 at t = .423 msec.

Peak displacement time history data is plotted on Figure 40 (these plotted values do not occur at the same point on the panel). This data shows a difference in initial response time followed by convergence toward the same peak displacement as t/T approaches 1.0. Error in the time synchronization could be responsible for part of the difference. Examination of the tested panel revealed that the actual impact was approximately one inch off the panel centerline. This is also responsible for a part of the difference in magnitude between the analytical and experimental results.

4.3.3 Oblique Impact ($\theta = 25°$)

a) Experimental Shot 40117

Analytical data was generated for the 25° oblique angle impacts using the loading model described in paragraph 3.1 of this report and in Reference 2. The impact mass (73.9g), velocity (129.5 m/sec), and 25° impact angle associated with this shot represent a low energy level impact condition.

The experimental and analytical results for the centerline displacement at successively increasing times are shown in Figures 41 through 44. The problem associated with travel of the deflected shape with time is again evidenced. The location of the peak deflection as measured experimentally moves from x = 68 mm at t/T = 0.088 to x - 8 mm at t/T = .46. The calculated peak displacement is stationary at x = 36 mm.

The peak panel displacement as a function of time is plotted on Figure 45. The experimental data presented in this plot is for a different panel location at each time as described in the preceeding paragraph. This data together with Figures 43 and 44 indicate a convergence (on inter-section) as t/T approaches 0.5.

---

[2] J. P. Barber, H. R. Taylor and J. S. Wilbeck, Bird Impact Forces and Pressures on Rigid and Compliant Targets. (AFFDL-TR-77-60, ADA061-313, May 1978.)

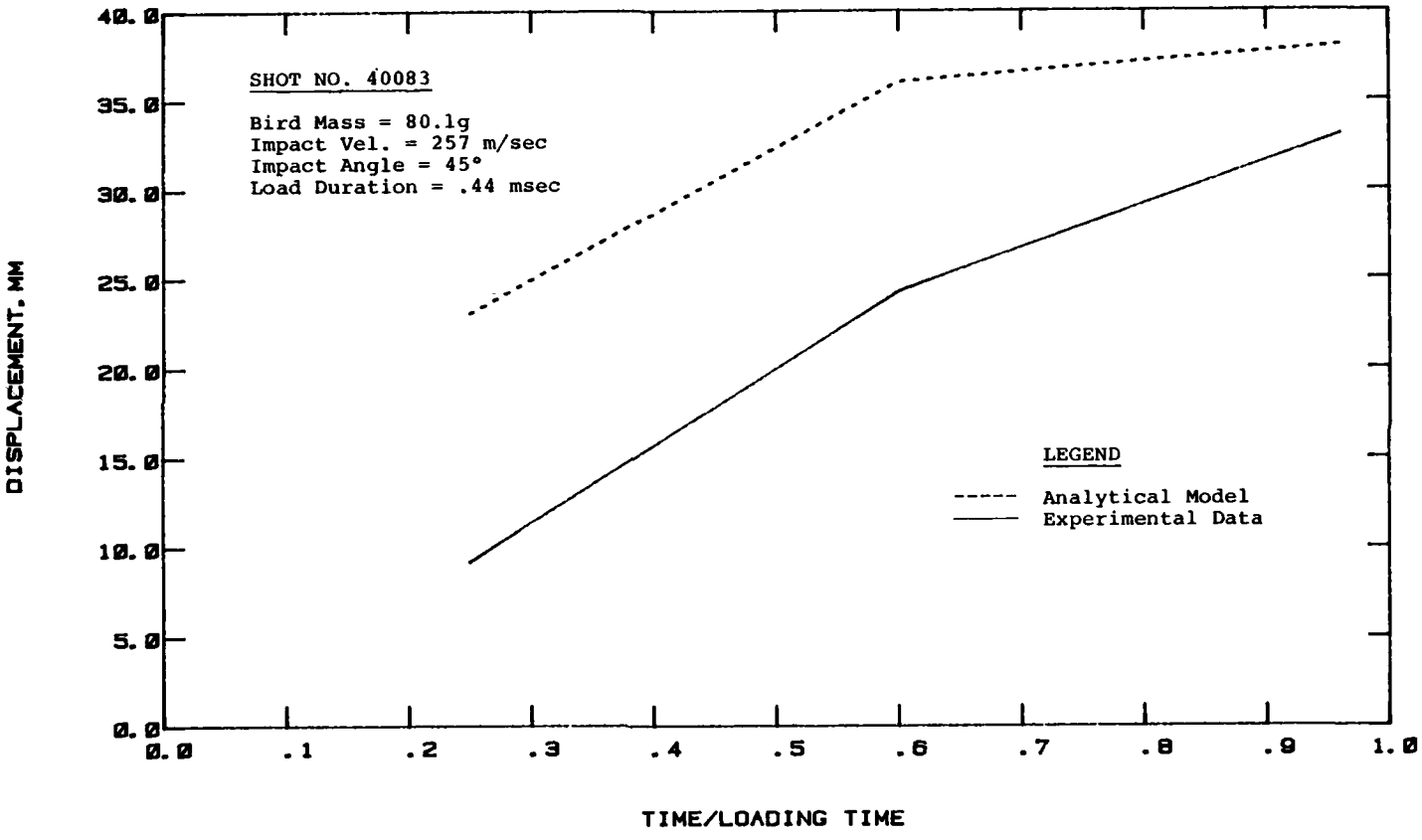

Figure 40. Comparison of Peak Panel Displacement vs. Time for Shot No. 40083.

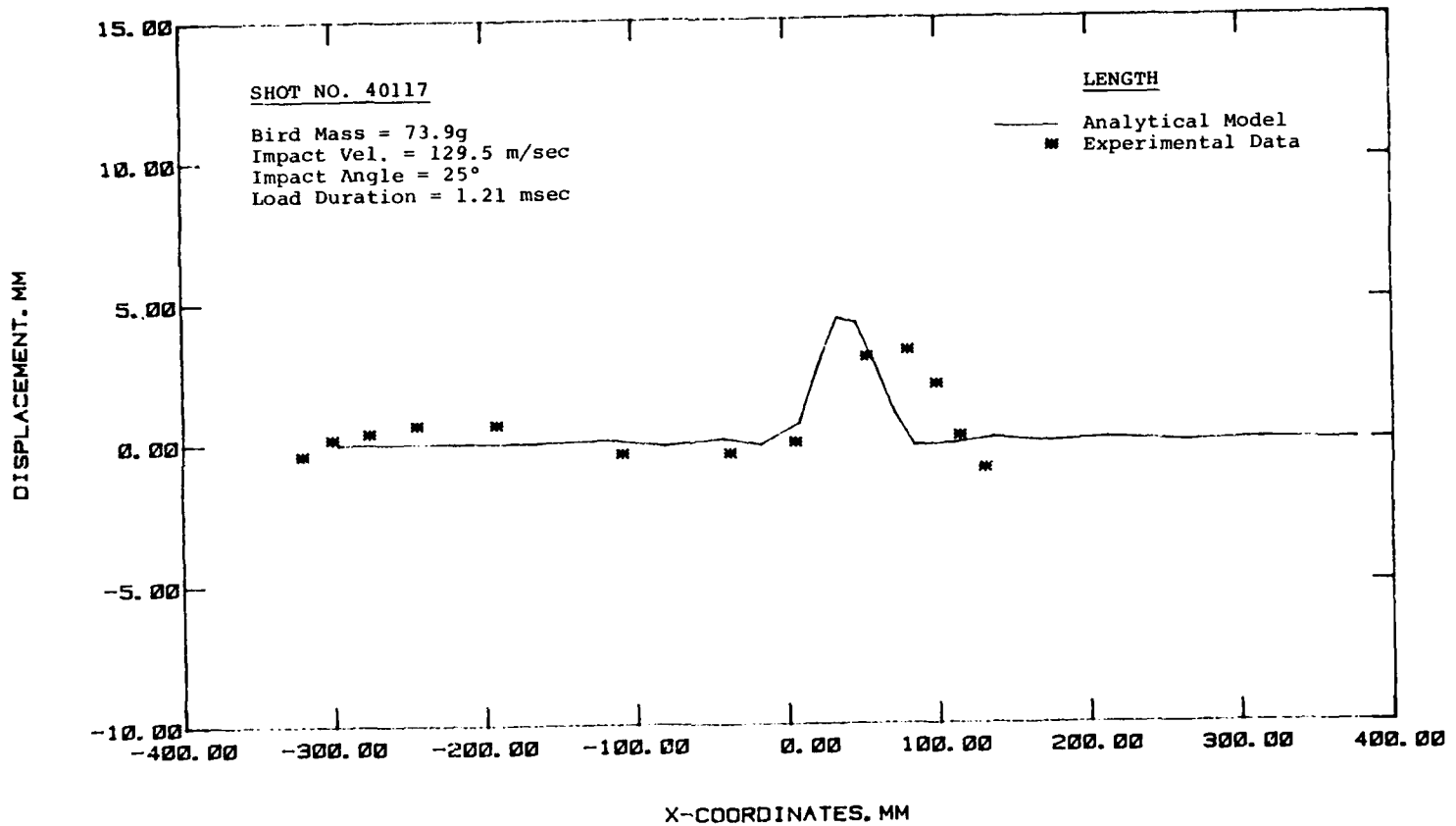

Figure 41. Comparison of Analytical and Experimental Results for Shot No. 40117 at t = 0.106 msec.

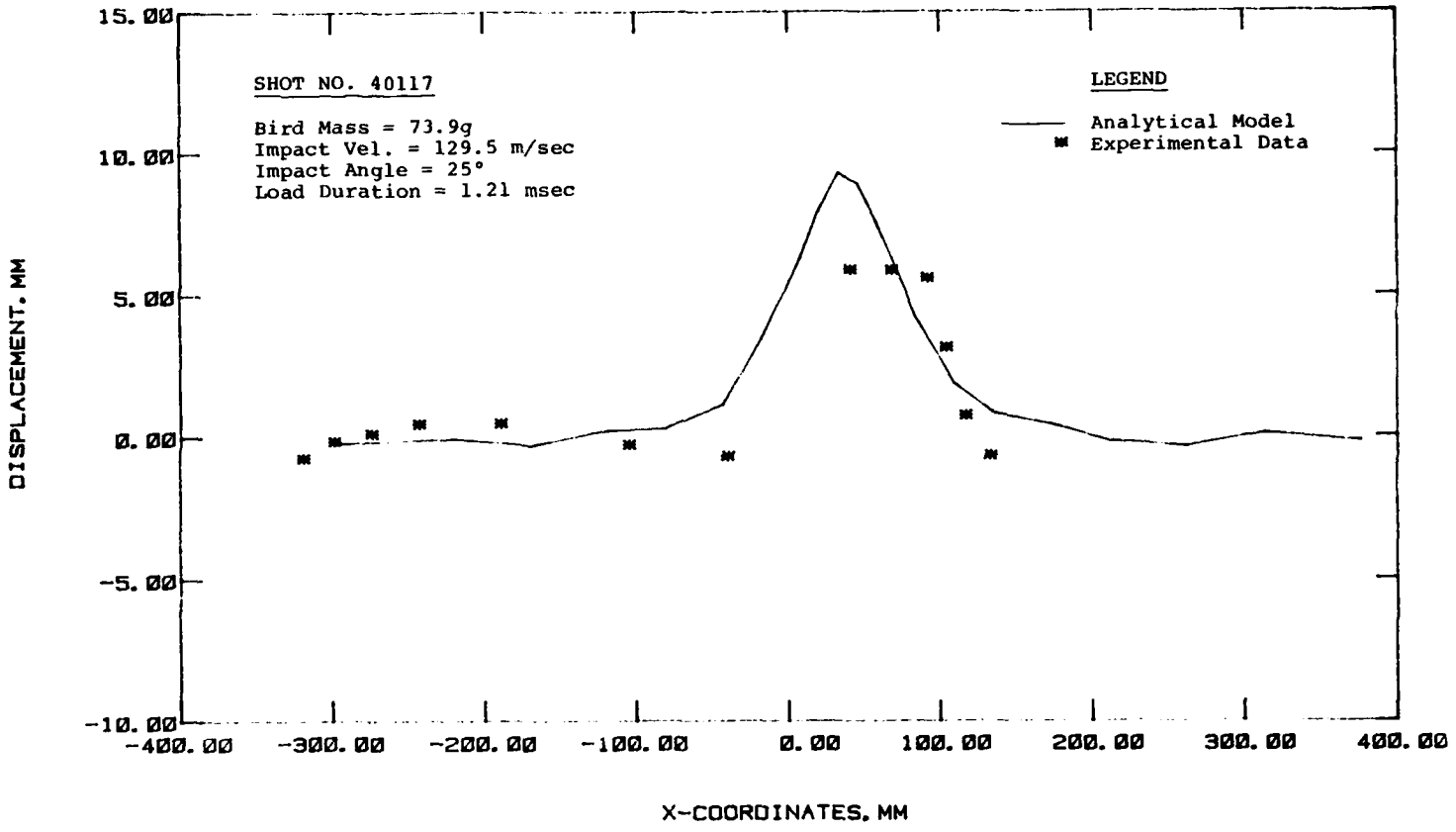

Figure 42. Comparison of Analytical and Experimental Results for Shot No. 40117 at t = 0.257 msec.

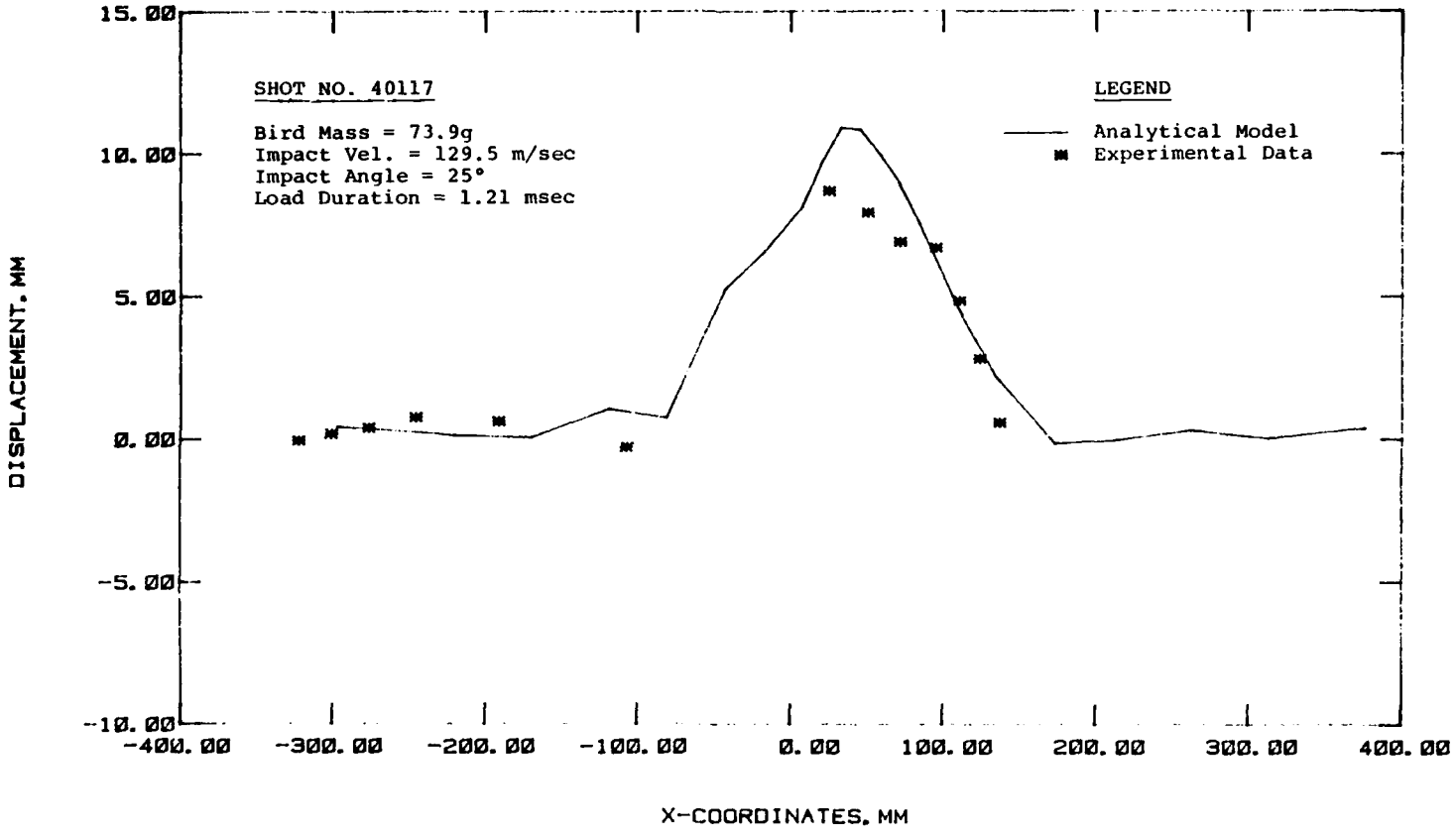

Figure 43. Comparison of Analytical and Experimental Results for Shot No. 40117 at t = 0.407 msec.

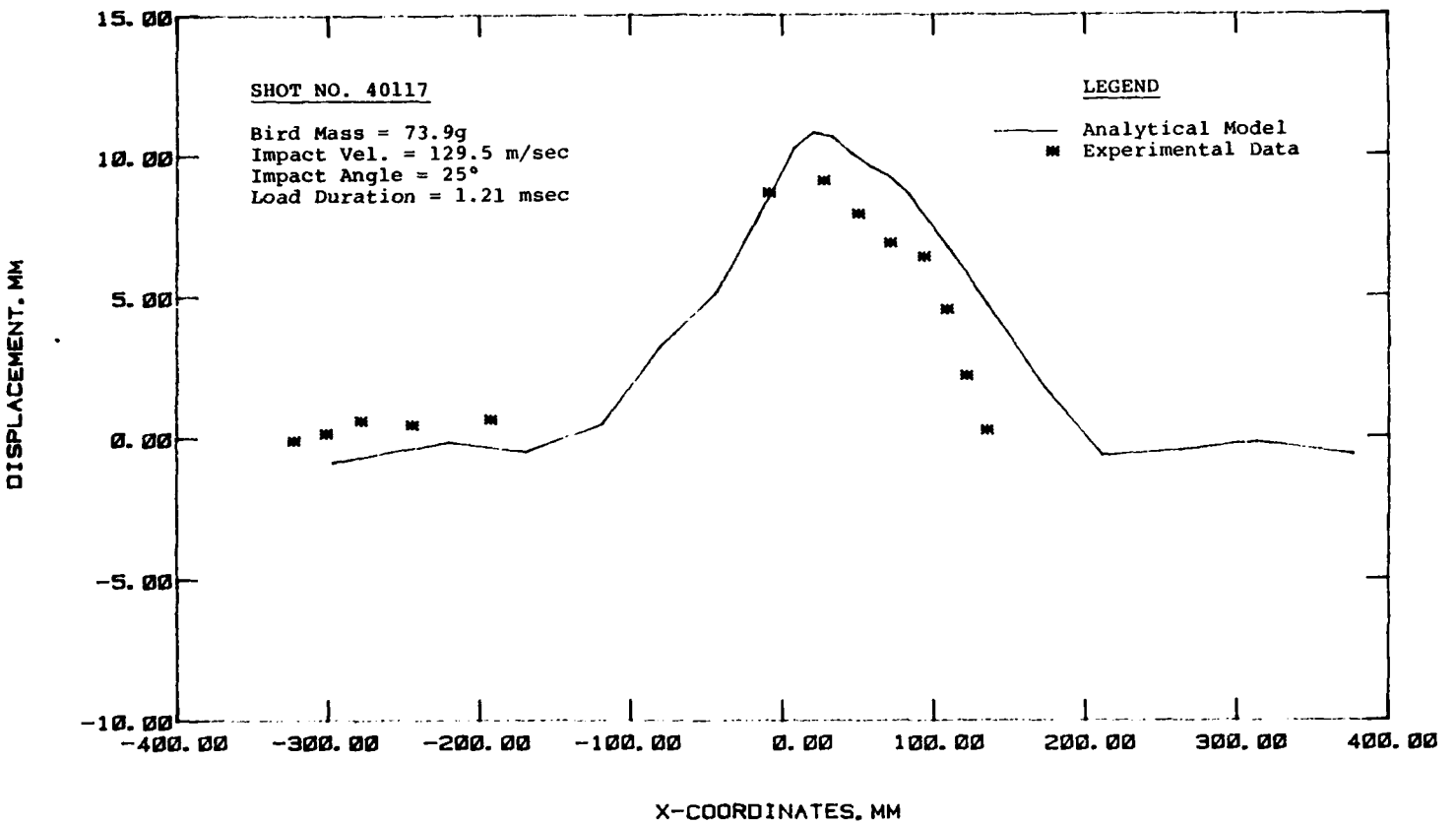

Figure 44. Comparison of Analytical and Experimental Results for Shot No. 40117 at t = 0.558 msec.

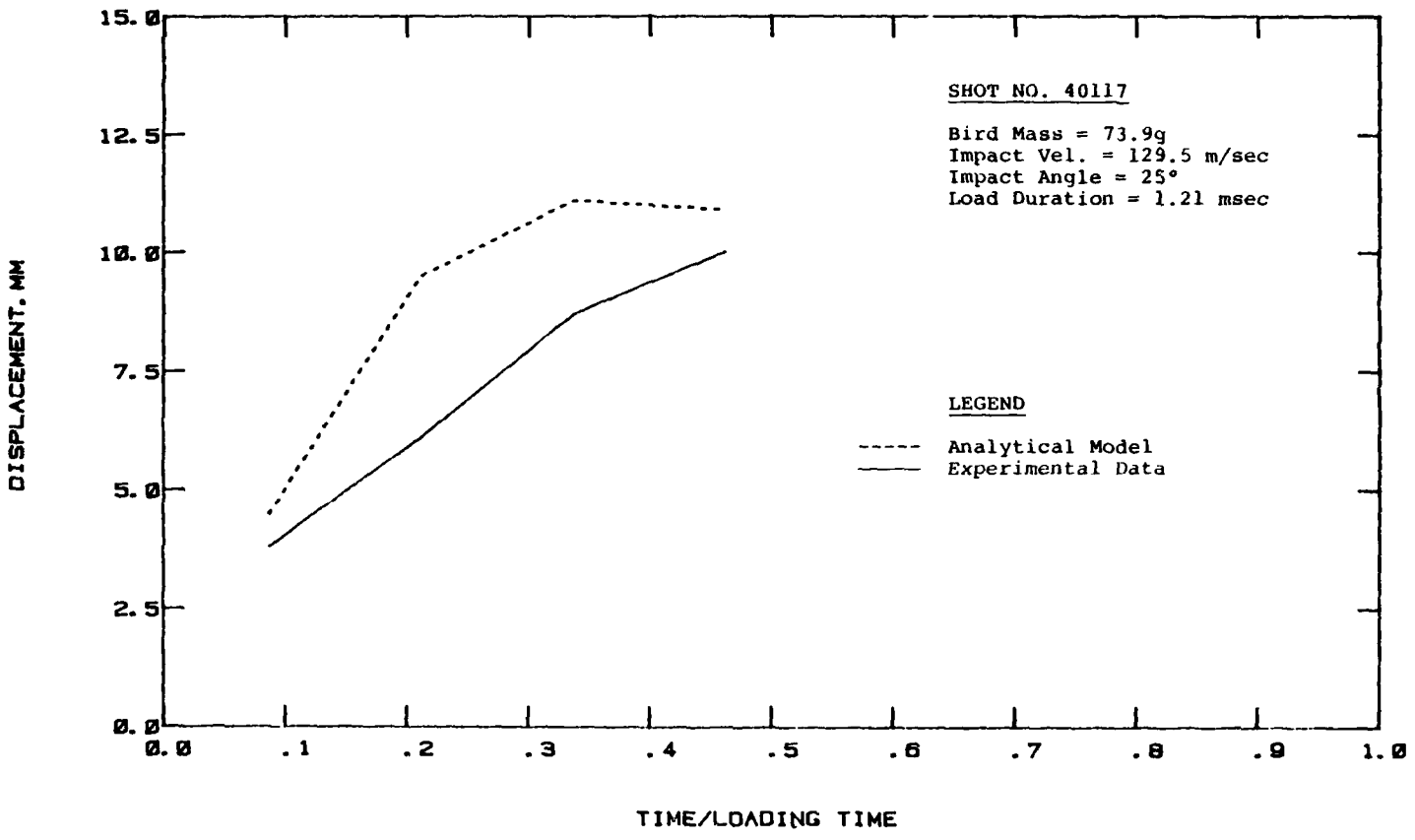

Figure 45. Comparison of Peak Panel Displacement vs. Time for Shot No. 40117.

b) Experimental Shot No. 40139

The impact mass (82.0g), the impact velocity (200 m/sec), and the 25° impact angle associated with this shot constitute an intermediate energy level impact. The maximum measured deflection was 17 mm at t/T = 1.47. The residual plastic pocket was about 7 mm in depth.

The experimental and analytical results for the centerline displacement at successively increasing times are shown in Figures 46, 47, and 48. The peak measured displacement moves from x = 25 mm at t/T = .096 to x = 3 mm at t/T = .490. The calculated peak displacement is stationary at x = 36 mm. The peak panel displacement as a function of time is presented on Figure 49 (these plotted values do not occur at the same point on the panel).

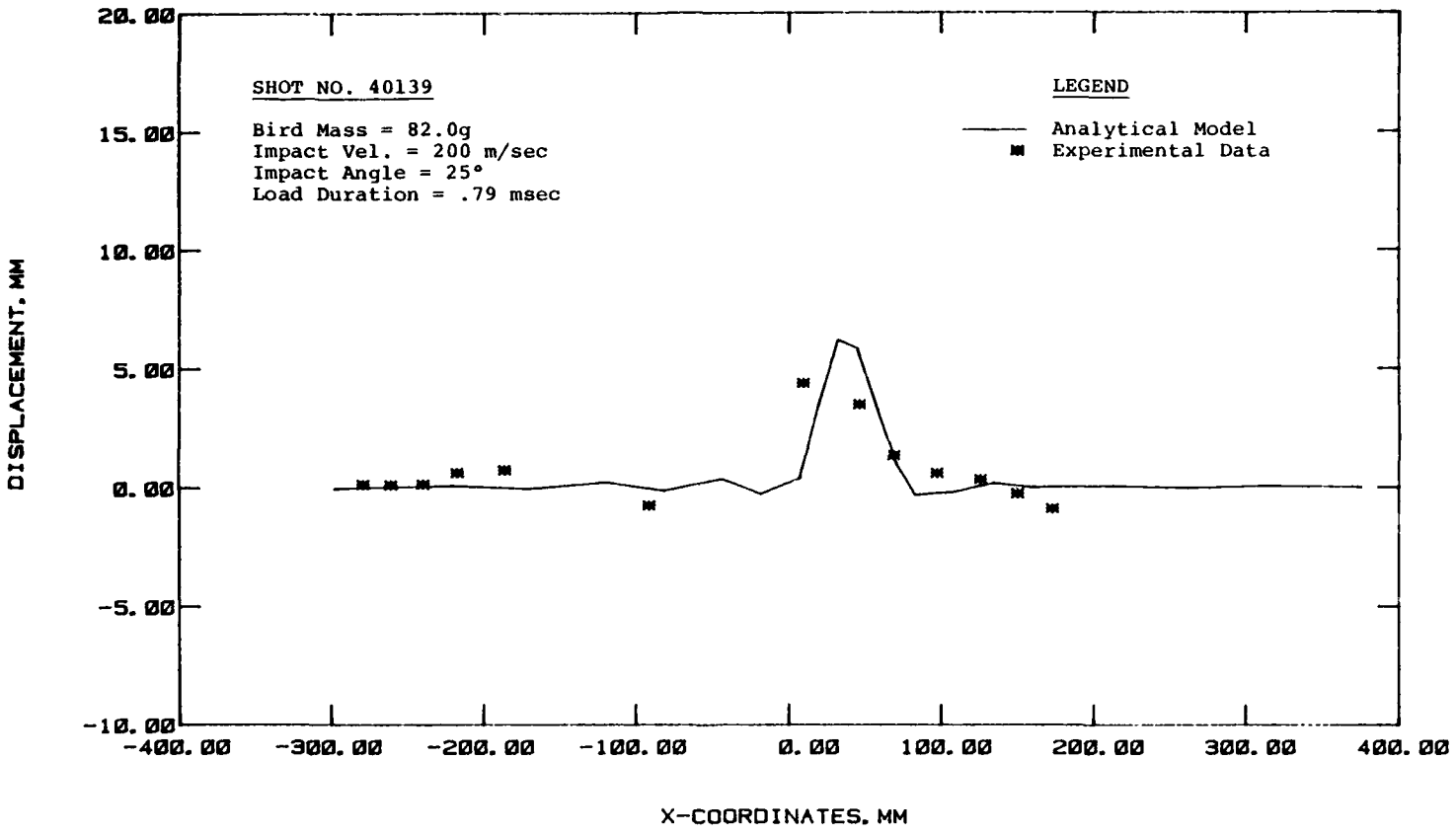

Figure 46. Comparison of Analytical and Experimental Results for Shot No. 40139 at t = 0.076 msec.

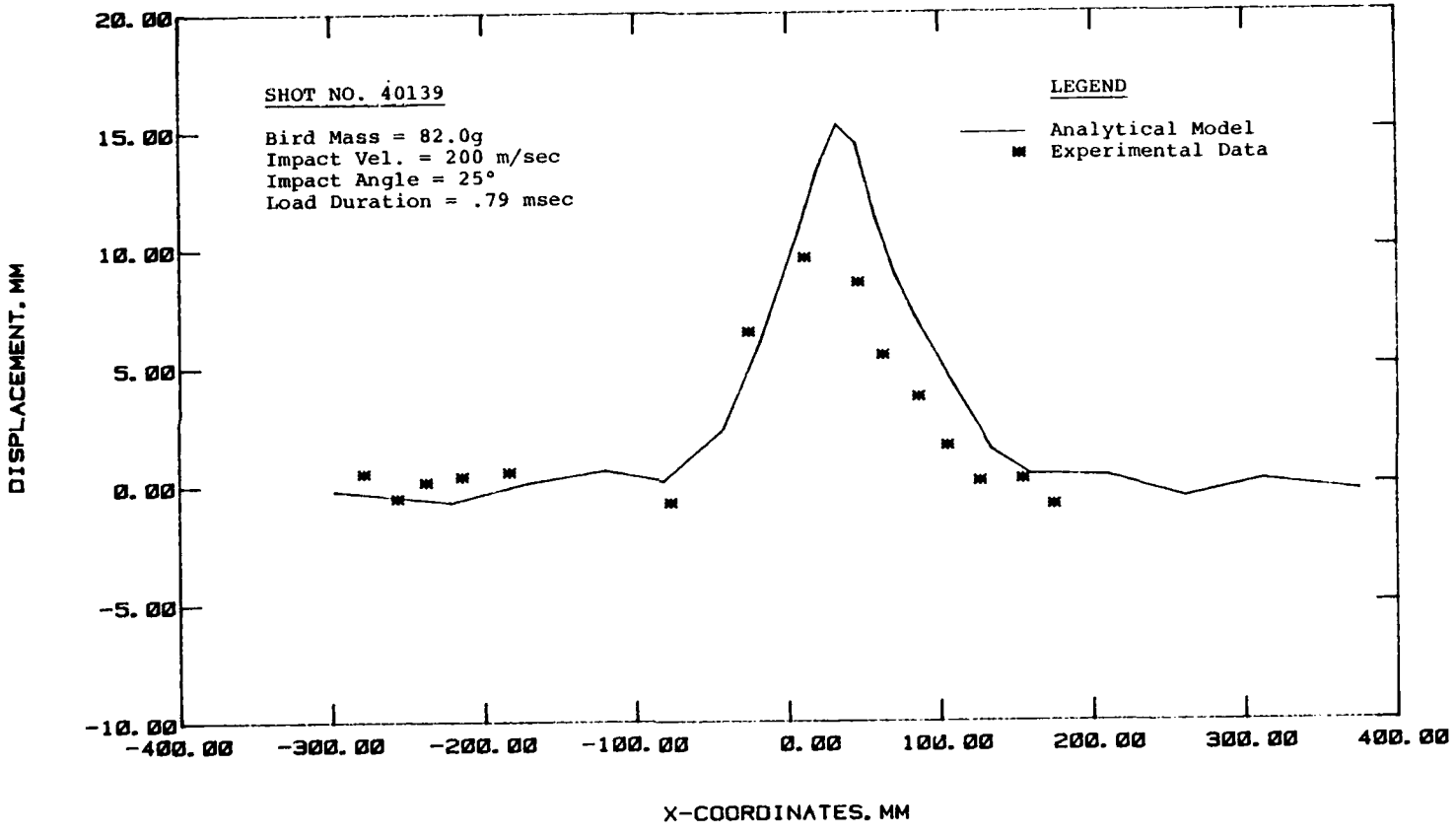

Figure 47. Comparison of Analytical and Experimental Results for Shot No. 40139 at t = 0.231 msec.

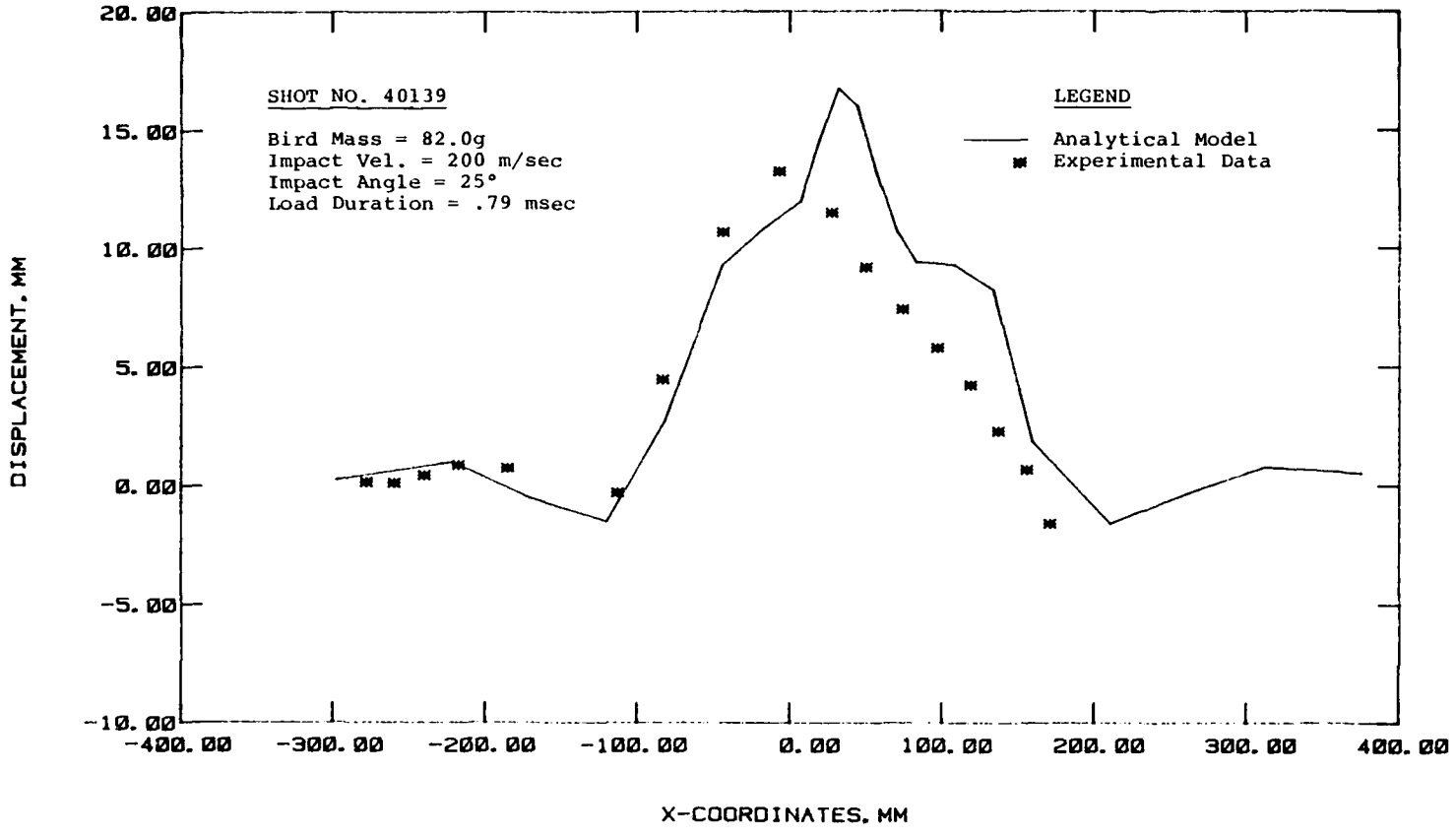

Figure 48. Comparison of Analytical and Experimental Results for Shot No. 40139 at t = 0.387 msec.

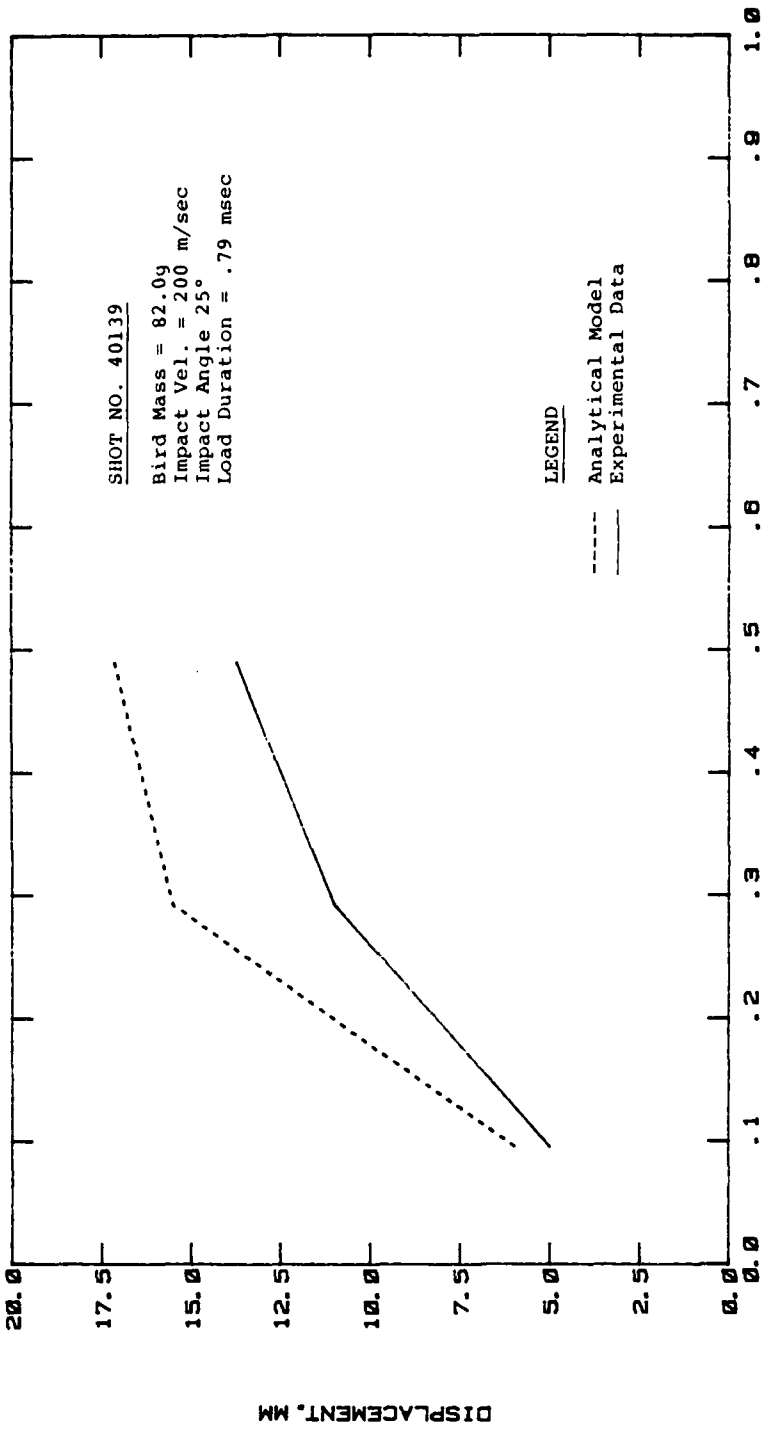

Figure 49. Comparison of Peak Panel Displacement vs. Time for Shot No. 40139.

SECTION 5
CONCLUSIONS AND RECOMMENDATIONS

The following conclusions are based on the results of this program and related experience.

1) The coupled load model of Reference 2, in its present formulation, is inappropriate for use with the MAGNA program for the design and analysis for bird impacts on aircraft windshield type structures.

2) Uncoupled loading models based on the data reported in Reference 2 can be used with MAGNA to analyze certain classes of structures under specified bird impact conditions. The amount of a priori information required to obtain good results is generally dependent on the complexity of the structural system and the nonlinearity of the response.

   By utilizing the existing data base, exercising good judgment, and introducing a degree of artificial coupling, useful analytical results are attainable for flat plates and aircraft transparency/support structure systems. Specifically, it is concluded that: (1) good results can be achieved for flat plates at normal impact; (2) by introducing artificial coupling to account for changes in load location with time good results can can be attained for oblique impact on flat plates and crew enclosure structures; (3) the amount of a priori information required to achieve good results for oblique impacts will increase with the nonlinearity of the response.

---

[2] J. P. Barber, H. R. Taylor, and J. S. Wilbeck, Bird Impact Forces and Pressures on Rigid and Compliant Targets. (AFFDL-TR-77-60, ADA061-313, May 1978.)

3) Analytical data generated with uncoupled loading models for the design of a new birdstrike resistant crew enclosure structure could not be used with a high level of confidence. Exceptions would be if the new system is structurally similar (nearly identical) to an existing system and/or the response level is to be only moderately nonlinear.

It is recommended that

1) A fully coupled load model be developed for use with the MAGNA program which would permit the design and analysis of bird impact resistant crew enclosure structures without any a priori knowledge.

2) Uncoupled load models based on the data presented in Reference 2 and prior experience (such as Reference 11) continue to be used to achieve a degree of artificial coupling until a fully coupled model can be effected.

3) Additional analytical studies be performed to further refine the load model for normal impact and to better characterize the load model for oblique impacts. This will provide a better data base for achieving artificial coupling until a fully coupled load model is available.

---

[2]J. P. Barber, H. R. Taylor, and J. S. Wilbeck, Bird Impact Forces and Pressures on Rigid and Compliant Targets. (AFFDL-TR-77-60, ADA061-313, May 1978.)

[11]R. E. McCarty, Finite Element Analysis of F-16 Aircraft Canopy Dynamic Response to Bird Impact Loading. (21st AIAA/ASME/ASCE/AHS Structures, Structural Dynamics, and Materials Conference, May 1980, Seattle, Washington.)

SECTION 6

REFERENCES

1. Barber, J. P., and Wilbeck, J. S., "The Characterization of Bird Impacts on a Rigid Plate: Part I," AFFDL-TR-75-5 ADA021142, January 1975.

2. Barber, J. P., Taylor, H. R., and Wilbeck, J. S., "Bird Impact Forces and Pressures on Rigid and Compliant Targets," AFFDL-TR-77-60, ADA061-313, May 1978.

3. Challita, A., and Barber, J. P., "The Scaling of Bird Impact Loads," AFFDL-TR-79-3042, June 1979.

4. Wilbeck, T. S., "Impact Behavior of Low Strength Projectiles," AFML-TR-77-134, July 1978.

5. Peterson, R. L., and Barber, J. P., "Bird Impact Forces in Aircraft Windshield Design," AFFDL-TR-75-150, ADA026-628, March 1976.

6. Brockman, R. A., "MAGNA: A Finite Element Program for the Materially and Geometrically Nonlinear Analysis of Three-Dimensional Structures Subjected to Static and Transient Loading," UDR-TR-79-45, October 1979.

7. West, B. S., "Design and Testing of F-111 Bird Resistant Windshield/Support Structure, Volume 1 - Design and Verification Testing," AFFDL-TR-76-101, October 1976.

8. Piekutowski, Andrew, J., "A Device to Determine the Out-of-Plane Displacement of a Surface Using a Moire' Fringe Technique," UDR-TR-79-58, 6 May 1979.

9. Bauer, David P., and Barber, John P., "Experimental Investigation of Impact Pressures Caused by Gelatin Simulated Birds and Ice," UDR-TR-78-114, March 1979.

10. Boehman, L. I., and Challita, A., "Model for Predicting Bird and Ice Impact Load on Structures," UDR-TR-79-54, February 1980.

11. McCarty, R. E., "Finite Element Analysis of F-16 Aircraft Canopy Dynamic Response to Bird Impact Loading," 21st AIAA/ASME/ASCE/AHS Structures, Structural Dynamics, and Materials Conference, May 1980, Seattle, Washington.

*U.S.Government Printing Office: 1980 — 657-084/179


DATE
ILME